Physics Reports 547 (2015) 1–24

Contents lists available at ScienceDirect

Physics Reports

journal homepage: www.elsevier.com/locate/physrep

Attosecond science and the tunnelling time problem

Alexandra S. Landsman *, Ursula Keller

Physics Department, ETH Zurich, CH-8093 Zurich, Switzerland

ARTICLE INFO

Article history:
Accepted 9 September 2014
Available online 28 September 2014
editor: J. Eichler

ABSTRACT

The question of how long it takes a particle to tunnel through a potential barrier has been a subject of intense theoretical debate for the last 80 years. In this decade of attosecond science, the answer to this question not only promises to deepen our understanding of fundamental quantum mechanics, but also has significant practical implications for how we interpret attosecond electron dynamics that underlie important phenomena in physics, chemistry and biology. Here we attempt to address this problem in the context of recent experimental measurements which use state-of-the-art ultrafast laser technology to resolve electron dynamics on the attosecond time-scale. This review therefore brings the theory of tunnelling time to the arena of ultrafast science, opening the door to improved resolution of, and cross-fertilization between, significant practical and fundamental questions in both fields.

Contents

1. Introduction 2
2. Strong field ionization: theory and experiment 2
   2.1. Relevant units and quantities in strong field ionization experiments 2
   2.2. Basic concepts 3
   2.3. Theoretical methods 4
   2.4. Strong field approximation 7
   2.5. Coulomb effects 9
   2.6. Times commonly arising in strong field ionization 10
3. Tunnelling time theory 12
   3.1. Definitions of tunnelling time 13
   3.2. Feynman path integral formulation for tunnelling time 15
   3.3. Tunnelling time definitions expressed as averaged values and weak measurement 17
4. Measurement of tunnelling time with the attoclock 18
   4.1. Prior experiments on tunnelling time 18
   4.2. Basic principle 19
   4.3. The experiment 20
   4.4. Comparison of experiment to theory 21
5. Conclusion 22
   Acknowledgements 23
   References 23

* Corresponding author. Tel.: +41 791291401.
E-mail address: landsmanster@gmail.com (A.S. Landsman).

http://dx.doi.org/10.1016/j.physrep.2014.09.002
0370-1573/

1. Introduction

The past decade saw an extraordinary evolution in experimental physics, aimed at the boundary between quantum and classical regimes, in the "real world" of atoms, molecules, and surfaces [1]. Ultrafast lasers and attosecond pulses have arrived, and with them comes attosecond science. The detailed measurement and resolution of, reconstruction of, and even active manipulation of the dynamics of valence electrons – and hence of real world chemistry in action – is at last becoming feasible [2–10]. These new experimental capabilities have both made more urgent and allowed to at last address the old, but still unresolved question of tunnelling time.

The tunnelling time problem is almost as old as quantum mechanics itself [11] and is a highly debated subject [12]. Time is not a quantum operator [13] and therefore many conflicting theories have been developed over decades [12–15], but definitive experiments until now were largely impossible, and awareness of the controversy in the broader scientific world faded. More recently, in the attosecond science community, tunnelling time is implicitly assumed to be deterministic and, very often, is posited to be instantaneous or imaginary [2,16,17]. Hence, even the high impact cutting-edge techniques for imaging valence electron dynamics in atoms and molecules are founded on instantaneous tunnelling [3–5].

On the other hand, it seems that the majority of the broader physics community has decades ago reached a consensus that tunnelling is not instantaneous. To quote Landauer: "The physics literature has, by 1993, largely accepted the fact that there is a time scale associated with the duration of the tunnelling process" [12]. Hence, there seems to be a sharp contrast, between, for instance, the discussion of tunnelling time in a condensed matter setting, where different tunnelling time definitions are debated with the underlying assumption that tunnelling time (whatever it is) is finite, and the attosecond science community where the default assumption is that it is instantaneous, and that moreover this view is both natural and uncontroversial. *It is the aim of this review to bring different communities together, combining experimental and theoretical expertise to shed new (ultrashort) light on the tunnelling time problem.*

Recent attempts at reconstructing valence electron dynamics in atoms and molecules have entered a regime where the tunnelling time genuinely matters [3–6]. Nevertheless, common reactions to tunnelling time can be roughly grouped into two categories: (1) it is easy or (2) it cannot be done. In the first category, it is sometimes suggested that the tunnelling time is instantaneous because both the Keldysh [18] and the closely related Büttiker–Landauer times [19] are imaginary (corresponding to the decay of the wavefunction under the barrier). However, both of these times were obtained using physical considerations of what a tunnelling electron actually sees in real time while inside the barrier [18,19]. In the "it can't be done" category, it is often said that quantum mechanical uncertainty does not allow for a deterministic tunnelling time. However, as we remind in this review, the main theoretical contenders for tunnelling time can be viewed as average values, rather than deterministic quantities [20–22].

Within the attosecond science community, the word "tunnelling time" is often used to denote very different physical phenomena, sometimes referring to the imaginary part of the ionization time [17] (which corresponds to the decay of the wave function under the barrier), sometimes to the time it takes to develop a constant outgoing flux [23], or, in one instance, to the phase of ionization [24]. Here, we focus on the traditional definition of tunnelling time, given in excellent reviews by Landauer and Martin [12] and by Hauge and Stovneng [14], among others, as corresponding to the real delay time that the electron experiences in traversing a physical barrier. Due to the non-classical dynamics of the electron, this tunnelling delay time is surprisingly difficult to formally define or measure and it is one of the goals of this review to give an idea of the variety of possible approaches to tunnelling time.

Tunnelling is the first crucial step in strong field ionization of atoms and molecules and underlies virtually all present-day experiments in attosecond science, such as High Harmonic Generation (HHG) [1]. Section 2 presents a brief overview of theory and experiment of strong field ionization, explaining both the basic mechanism and some of the still unanswered questions about the tunnelling process itself. Perhaps the most important and fundamental of these open questions, tunnelling time, is presented in Section 3. Section 4 describes the use of the attoclock [9,22,25,26] for measuring tunnelling delay time, and discusses recent experimental measurements. Section 5 summarizes the implications of non-instantaneous tunnelling time on the field of attosecond science, the current status of the tunnelling time question, and points to the still unanswered questions and further directions of research, both with practical and fundamental aims.

2. Strong field ionization: theory and experiment

Here we introduce basic concepts of tunnel ionization, in particular how to interpret electron momenta distributions at the detector. We will refer frequently to these concepts in the following sections, when we introduce the concept of the attoclock and relate experimental observables, such as the one shown in Fig. 1b, to tunnelling time. We will also explain how Keldysh time arose as a candidate for tunnelling time and its close connection to the Büttiker–Landauer time, commonly mentioned in the tunnelling time literature.

2.1. Relevant units and quantities in strong field ionization experiments

Throughout this review, we will use atomic units (au). In au units, $\hbar = m = e = 1$, where m and e are mass and charge of the electron, respectively. In deriving analytic expressions, we will therefore often drop $\hbar$, m and e values from the formulas,

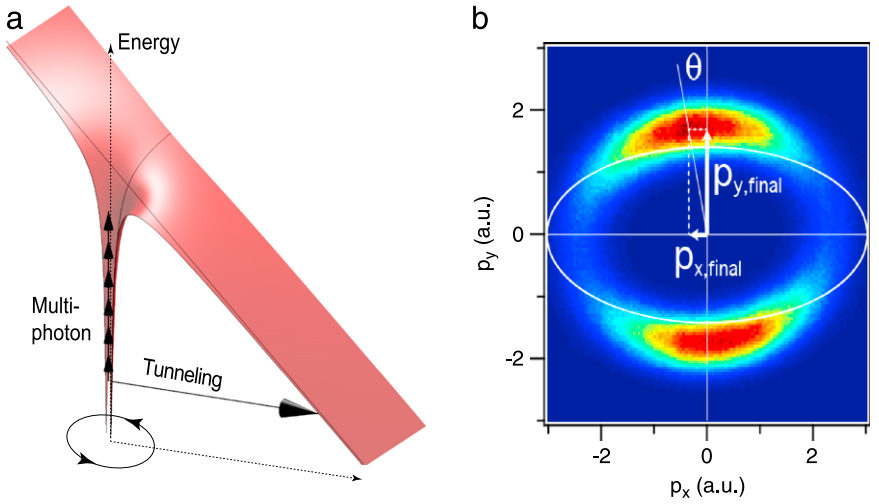

Fig. 1. Strong field ionization, taken from [28]. (a) The combined potential created by the Coulomb field of the atom and the laser field. The electron can escape the atom either by tunnelling (horizontal channel) or multi-photon ionization (vertical channel). (b) Electron momenta distributions measured at the detector after strong field ionization for close-to-circularly polarized light of ellipticity, $\epsilon = 0.87$.

as is often done in the strong field ionization literature [27]. Atomic units are particularly convenient in theoretical modelling, making it easy to compare and assign relative importance to the various forces acting on the electron. For example, the force binding the electron to the helium atom is of $\sim O(1)$ au at the Bohr orbital radius, while the electric field of the laser at typical experimental intensities is about $F = 0.04$–0.1 au [22]. Therefore, while the electron is bound inside the atom, the Coulomb force is much stronger than the laser field and the electron can only escape via the process of tunnelling or multi-photon ionization. On the other hand, after the electron appears at the tunnel exit (a distance of order of 10 au, depending on ionization potential and laser parameters), the Coulomb field is weak compared to the laser field strength, and the electron dynamics follow, to the lowest order, the electric field of the laser only.

Another relevant parameter is the laser centre wavelength frequency, ω, which in the IR range (wavelength 700–1000 nm) is around 0.0456–0.065 au; a much slower time-scale than the oscillation frequency, ω_e, of the electron inside the atom (also $\sim O(1)$ au), or $\omega_e \gg \omega$. This means that for a bound electron, the time-dependent field varies adiabatically, leading to more analytically tractable dynamics [29,30]. The $\omega_e \gg \omega$ adiabatic condition is expected to break down in the case of larger molecules, where the time-scale of electron motion becomes comparable to the laser field [31]. Below, we introduce another important parameter widely used to measure the degree of non-adiabaticity in tunnel ionization: the Keldysh γ [18].

2.2. Basic concepts

Strong field laser ionization involves two crucial steps that beautifully combine classical and quantum mechanics: First, the electron is freed from the atom either via **tunnel** or **multi-photon** ionization [32], as shown in Fig. 1a. Next, it propagates classically in the combined ion–laser field, after which it either rescatters, resulting in processes like double ionization [33] or high harmonic generation (HHG) [34], or it gets away from the parent ion, registering its momentum at the detector (see Fig. 1b). The two ionization channels can be identified as vertical (for multi-photon) and horizontal (for tunnelling) ionization channels [27]. In tunnelling, the combined Coulomb–Laser field forms a potential barrier, through which the electron tunnels without absorbing quanta of energy from the field. On the other hand in the multi-photon regime, the electron sees a quickly oscillating electric field and absorbs many photons, n, thereby gaining enough energy to go over the potential barrier when $\hbar\omega n > Ip$. *While tunnel ionization has a preferred direction of emission*, namely the direction of the instantaneous electric field, *multi-photon ionization is believed to be independent of the phase of the laser field* [35], since the electron escapes by going over the top of the potential well (see Fig. 1a). By far, the majority of phenomena in attosecond science rely on the concept of tunnel ionization. For example, the reconstruction of valence electron dynamics inside a molecule rests on the assumption that the direction of electron emission is determined by the direction of the instantaneous electric field, thereby necessitating the tunnelling picture in order to map out the density of the bound electron wavefunction [3,7,8].

Tunnel and multi-photon ionization regimes are separated by the Keldysh parameter,

$$\gamma = \omega \frac{\sqrt{2I_p}}{F} = \sqrt{\frac{I_p}{2U_p}} \tag{1}$$

where I_p is the ionization potential, U_p ponderomotive energy, ω is the laser frequency, and F is the strength of the electric field at the instance of ionization. The tunnelling regime is then defined by $\gamma \ll 1$, whereas the multi-photon ionization

regime is $\gamma \gg 1$, with the 'cross-over' region being $\gamma \sim 1$. These two regimes can be intuitively understood by considering the two laser parameters that determine γ in Eq. (1): frequency, ω, and field strength, F. At higher laser frequency (corresponding to higher γ), the electron needs to absorb less photons to overcome the binding potential, hence multi-photon ionization pathway (or the vertical channel in Fig. 1a) is more likely. On the other hand, at higher field strengths (corresponding to lower γ), the probability of tunnelling increases exponentially, since the barrier width is given approximately by I_p/F. Hence, the tunnelling mechanism (or the horizontal channel in Fig. 1a) dominates. It is the interplay of these two laser parameters, which together determine γ, that decides the relative contributions of tunnelling and multi-photon ionization pathways.

The experiments today operate close to the cross-over regime, with majority falling in the γ equal to 0.5–1.5 range, depending on the ionization potential of the sample, laser frequency and intensity (see for example [3,2,36,37]). For instance, a typical laser experiment using an ultrafast Ti:Sapphire laser (pulse duration anywhere between around 5–50 fs), with a peak intensity of 3×10^{14} W/cm^2 in the wavelength of 735 nm, results in a Keldysh parameter $\gamma \approx 1.2$ for ionization of Helium gas [22]. Hence, today's experiments are believed to operate in the regime of *non-adiabatic tunnelling* [35], where some multi-photon absorption occurs, but tunnelling remains the dominant ionization mechanism, even, as some experiments indicate [6], for γ as high as $\gamma = 3$. To sum up, as γ increases, the dynamics are believed to start to deviate from adiabatic (or quasi-static) limit, which holds for $\gamma \ll 1$, to non-adiabatic tunnelling, to multi-photon ionization for $\gamma \gg 1$.

2.3. Theoretical methods

A number of non-adiabatic tunnelling theories have been developed [38–41], many of them building on the seminal work by Perelomov, Popov and Terentev (PPT) [42,43]. These methods are based on the approximate solution of the Schrödinger equation and the subsequent application of the saddle point analysis or the imaginary time method [43,44]. This method uses sub-barrier trajectories in imaginary time to calculate ionization probabilities, where the sub-barrier trajectories can be obtained using the saddle-point method. While such trajectories have proven an extremely useful analytic tool in evaluating transmission probabilities, they are less suitable for evaluating phase-dependent tunnelling times, predicting instantaneous tunnelling. This will be discussed in more detail in Section 4.

In the adiabatic ($\gamma \ll 1$) limit, PPT can be shown to reduce to a popular theory developed by Ammosov, Delone and Krainov (ADK) [45]. Both PPT and ADK theories are based on the important underlying assumption, arising from the Strong Field Approximation (see below) that the Coulomb field of the parent ion can be neglected after the electron appears at the tunnel exit. This is because the Coulomb field is relatively weak compared to the strong field of the laser, and therefore does not substantially alter electron dynamics after ionization. Long-range Coulomb potential can nevertheless be taken into account by performing Classical Trajectory Monte Carlo (CTMC) simulations [36,41,46,47] or analytically by using perturbation theory [44]. In CTMC simulations, trajectories are launched using the initial conditions based on the ionization probabilities obtained either from PPT or ADK. These two theories have different predictions for the initial velocity at the tunnel exit point, as well as the location of the tunnel exit point itself. In particular, ADK predicts that the most probable initial electron momentum at the tunnel exit is zero, and the transverse velocity distribution, $\mathbf{v}_\perp$, (or distribution perpendicular to the direction of tunnelling) is given by [45,48]:

$$|\langle \mathbf{v}|\Psi\rangle|^2 \propto \exp\left(-\frac{2\left(2I_p\right)^{3/2}}{3F}\right)\exp\left(-v_\perp^2\frac{\sqrt{2I_p}}{F}\right) \tag{2}$$

where Ψ is the single active electron wave function. When ADK theory is applied, the adiabatic tunnel exit point obtained in the short-range potential approximation, or $x_e = I_p/F$, is frequently used [41,49]. Alternatively, an exit point obtained by solving the equation: $-I_p = -1/x - Fx + v^2/2$, with velocity set to zero, is also used [50], resulting in an exit point referred to as the Field Direction Model (FDM) [26] and given by,

$$x_{e,f} = \frac{I_p + \sqrt{I_p^2 - 4F_{max}}}{2F_{max}} \tag{3}$$

where $F_{max} = F_0/\sqrt{\epsilon^2+1}$ is the maximum electric field.

The experimental data as seen at the detector (Fig. 1b) can be qualitatively reproduced by launching CTMC simulations (shown in Fig. 2 for different ellipticities of laser light) at the tunnel exit with zero velocity in the direction of tunnelling, and with transverse velocity distribution, $p_\perp$ given by Eq. (2). Each electron trajectory then follows classical equations of motion, given by the field of the parent ion, and the strong laser field, where the laser field is commonly approximated as [34]:

$$\mathbf{F}(t) = \frac{-F_0 f(t)}{\sqrt{\epsilon^2+1}}[\cos(\omega t + \phi_c)\,\hat{x} + \epsilon \sin(\omega t + \phi_c)\,\hat{y}] \tag{4}$$

where ω is the central frequency of the laser, ϵ is the ellipticity (the major axis of polarization is along $\hat{x}$), and $f(t)$ is the slowly-varying pulse envelope: $f_{max} = f(0) = 1$. For many-cycle pulses, we can approximate the carrier-envelope offset

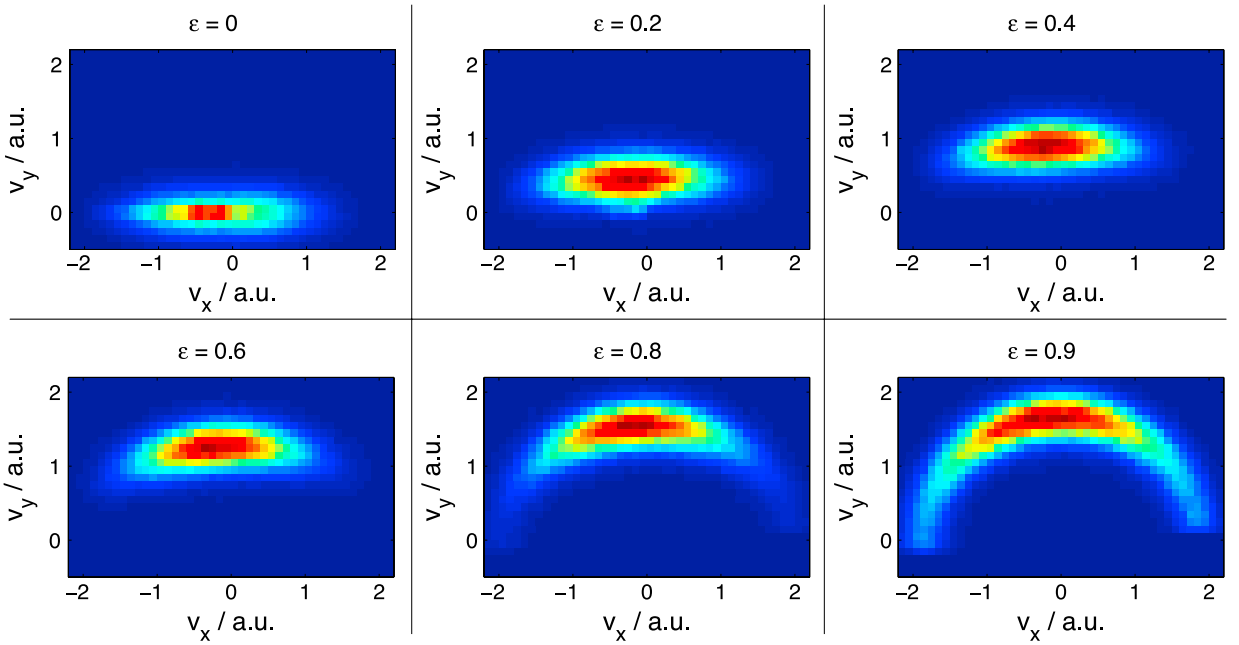

Fig. 2. Classical Trajectory Monte Carlo (CTMC) simulations using a TIPIS model [26] for different ellipticities of laser light, taken from [46]. Only one of the two symmetric lobes is shown.

(CEO) phase [51]: $\phi_c \approx 0$. In the following discussion, we shall set $\phi_c = 0$, corresponding to the peak of the electric field occurring at $t = 0$.

Note that the field given by Eq. (4) is an electric field only, hence neglecting the transverse magnetic component. This arises from the use of the *dipole approximation*, which neglects the spatial dependence of the laser field, since the wavelength of the IR laser is much longer than the excursion distance of the ionized electron during the duration of the pulse, leading to: $\mathbf{B} = \nabla \times \mathbf{A} \approx 0$. The use of the dipole approximation considerably simplifies the dynamics, and is key behind the use of the tunnelling picture in strong field ionization. For higher laser intensities, above 10^{16} W/cm^2, magnetic field effects become significant, necessitating different type of analysis [43,52–55] and HHG is suppressed due to the perpendicular drift introduced by the B-field [56].

The tunnelling picture follows after expressing the potential due to the laser field in the length-gauge formulation as: $V(r) = \mathbf{r} \cdot \mathbf{F}(t)$. The short range-potential approximation assumes that the long (slowly varying for $r \gg 1$) tail of the Coulomb potential can be approximated as a flat horizontal line inside the potential barrier. In this case, the length-gauge Hamiltonian in the short-range potential approximation [27,49] can be expressed as,

$$\hat{H}_{LG} = \frac{\hat{p}^2}{2} + \mathbf{r} \cdot \mathbf{F}(t) \tag{5}$$

where $\hat{p}$ denotes the kinetic momentum of the electron (equal to velocity in atomic units), and $\mathbf{F}(t)$ is the field strength, given by Eq. (4). The adiabatic tunnel exit point at the peak of the laser field can be obtained from Eq. (5) by setting the kinetic energy term equal to zero and energy to $-I_p$, resulting in: $x_e = I_p/F_{max}$, where $F_{max} = F_0/\sqrt{\epsilon^2 + 1}$.

A more accurate adiabatic semi-classical model that fully incorporates the $1/r$ potential can be obtained by changing into parabolic coordinates [26,57]. In this case, the Schrödinger equation for a single electron in the $1/r$ potential and a static external electric field separates [57], and the exit point can be approximated as [46]:

$$x_{e,p} \approx \frac{I_p + \sqrt{I_p^2 - 4\beta F_{max}}}{2F_{max}} \tag{6}$$

where $\beta = 1 - \sqrt{2I_p}/2$. The parabolic exit point has been used as an initial condition in the CTMC simulations combined with the ADK probability distribution for the initial electron momenta to obtain electron momenta distributions, such as the one shown in Fig. 2, which were in good agreement with experimental data in [26], particularly after accounting for the dipole interaction term in Argon (the dipole term was found to have a negligible effect in Helium). This approach of using an exit point given approximately by Eq. (6), ADK probability distribution for the initial velocities, and taking account of a higher order dipole term in the classical equations of motion is known as the **TIPIS model** [26]. TIPIS is expected to work best in the low frequency, high laser intensity limit, when γ is small: $\gamma \ll 1$. At higher values of γ, some multi-photon absorption is expected to occur. In this regime, TIPIS (which assumes a static electric field and hence a purely tunnelling process) may

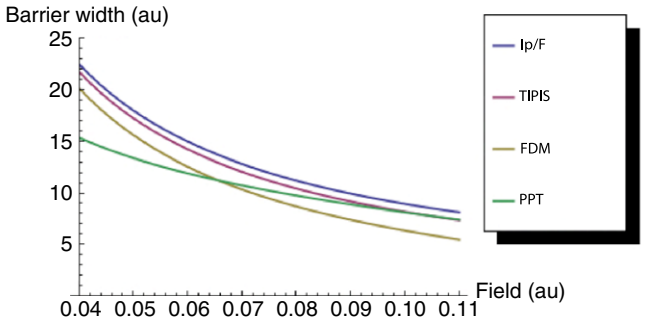

Fig. 3. Barrier widths predicted by different models: PPT, TIPIS, and FDM (field-direction model), taken from [28]. At high field strengths, corresponding to $\gamma \ll 1$, the PPT curve approaches the I_p/F curve.

be less reliable. *We will come back to both TIPIS and PPT models in the context of extracting tunnelling time from the attoclock measurements*. For convenience of presentation, we will refer to the exit point given by Eq. (6) as the TIPIS exit point, even though it already directly follows from the application of widely used parabolic coordinates, with excellent exposition given in Landau and Lifshitz [57].

An alternative to using a TIPIS model, which is expected to break-down at lower intensities (although some recent work finds that TIPIS may hold at much lower intensities than expected [32]), is to use a γ-dependent non-adiabatic approach that follows from the imaginary time method [42,44]. In this case, the tunnel exit is obtained from the complex valued sub-barrier trajectories obtained using the saddle-point approach [38,43,44]. The exit point in this case depends on the non-adiabaticity parameter, γ, approaching the ADK adiabatic exit point, I_p/F, in the $\gamma \ll 1$ limit [42]:

$$x_{e,na} = \frac{F_{max}}{\omega^2}\left(ch\left(\omega\tau_0\right) - 1\right) \tag{7}$$

where τ_0 solves the following equation [38,42]

$$\sinh^2\tau_0\left[1 - \epsilon^2\left(\coth\tau_0 - \frac{1}{\tau_0}\right)^2\right] = \gamma^2. \tag{8}$$

Fig. 3 compares barrier widths predicted by the three different theories: ADK, PPT, and TIPIS. As can be seen, there is only a small difference between the TIPIS (magenta curve, Eq. (6)) and the I_p/F (blue) widths. Moreover, the PPT (green curve, Eq. (7)) barrier width approaches I_p/F at smaller values of γ, corresponding to higher field strengths, but substantial deviations occur at higher γ, indicating that non-adiabatic effects become significant at lower laser intensities. The fourth curve (yellow–green, Eq. (3)) corresponds to the exit point given by the field direction model [26], and shows somewhat significant differences from the $x_{e,p}$ exit point, which is a more accurate solution of the combined Laser–Coulomb potential in the adiabatic limit. Therefore, in the adiabatic model, either I_p/F or $x_{e,p}$ exit points can be used, while in the non-adiabatic regime, the PPT exit point given by Eq. (7) can be employed. In addition to differences in the exit point, there is a difference in the initial velocities at the tunnel exit between adiabatic and non-adiabatic predictions. Indeed, it is this difference which is often referred to as distinguishing adiabatic from non-adiabatic regimes [2,32]. The centre of the electron momenta distribution at the tunnel exit is equal to zero according to adiabatic prediction. This can be clearly seen in Eq. (2), where $|\langle\mathbf{p}|\Psi\rangle|^2$ is maximized when $p_\perp = 0$. This differences in initial velocities results in differences in the final momenta distributions found at the detector. In particular, neglecting the higher-order Coulomb correction, the final momentum at the detector corresponds to conserved canonical momentum, which is given by:

$$\mathbf{P} = \mathbf{v}(t_0) - \mathbf{A}(t_0) \tag{9}$$

where t_0 can be the instance the electron appears at the tunnel exit and $\mathbf{A}$ is the vector potential of the laser field. The equivalence between conserved canonical momentum and final momentum at the detector comes about because at the time, t_{final}, when the electron is registered at the detector, the laser pulse has already passed: $\mathbf{A}(t_{final}) \approx 0$, resulting in: $\mathbf{P} = \mathbf{v}(t_{final})$.

Eq. (9) comes directly from conservation of canonical momentum that arises whenever spatial dependence is absent in the Hamiltonian: $dP/dt = -\partial H/\partial r = 0$. In this case the time-dependent Hamiltonian is given by the kinetic energy of the electron,

$$H_F(t) = \frac{1}{2}v(t)^2 = \frac{1}{2}[\mathbf{P} + \mathbf{A}(t)]^2 \tag{10}$$

where the subscript F denotes that only the laser field is included in the Hamiltonian. Eqs. (9) and (10) are only strictly valid for short-range potentials, where we can neglect the $V(r)$ term for $r \geq x_e$. The long-range potential of the parent ion introduces small, but noticeable corrections to this final momentum, which will be described in Section 2.4.

Table 1
Theoretical predictions of initial conditions at tunnel exit.

Theory	Type	r_{exit}	v_{initial}
ADK	Adiabatic	I_p/F	0
FDM	Adiabatic	$x_{e,f}$, Eq. (3)	0
TIPIS	Adiabatic	$x_{e,p}$, Eq. (6)	0
PPT	Non-adiabatic	$x_{e,na}$, Eq. (7)	$p_{na}(0)$, Eq. (12)

Despite its approximate nature, Eq. (9) has been used frequently for attosecond angular streaking [1,7] to time the moment that the electron appears at the tunnel exit from observing its final momentum at the detector. In the adiabatic regime, the most likely electron trajectory appears at the tunnel exit at the peak of the electric field, at a time $t_0 = 0$ (see Eq. (4)) with zero initial velocity, assuming field intensity is sufficiently low that no saturation or over-the-barrier ionization occurs. This results in the final momentum, given approximately by:

$$\mathbf{P}_{adiab} = \pm\mathbf{A}(0) = \pm\frac{\epsilon F_0}{\omega\sqrt{\epsilon^2+1}}\hat{y} \tag{11}$$

where we have used Eqs. (4) and (9) with $\mathbf{p}(0) = 0$ and $\mathbf{F} = -\partial\mathbf{A}/\partial t$. Eq. (11) corresponds to the location of the centre of the electron momenta distribution for elliptically polarized light with major axis of polarization along the x-axis, such as shown in Eq. (4). The approximate validity of this equation can be verified by looking at Fig. 1b, which shows that the electron momenta distributions are predominantly displaced along the y-axis. The additional angular rotation, which results in a non-zero momentum component along the x-axis, labelled as $P_{x,final}$ in the figure, will be discussed in Section 2.4.

In the non-adiabatic regime, the final momentum of the centre of the distribution is likewise predicted to point along the minor axis of polarization (neglecting Coulomb effects), but is displaced higher than the adiabatic case. This is due to a non-zero velocity offset at the tunnel exit, given by complex-valued trajectories that follow from the imaginary-time method by [38,42,44],

$$\mathbf{p}_{na}(0) = \frac{\epsilon F_0}{\omega\sqrt{\epsilon^2+1}}\left(\frac{\sinh(\tau_0)}{\tau_0} - 1\right)\hat{y} \tag{12}$$

where τ_0 is determined from Eq. (8). Note that, in contrast to Eq. (2), the momentum spread at the tunnel exit is centred around $\mathbf{p}_{na}(0)$, rather than zero. The prefactor and the standard deviation is also somewhat larger, and can be found in [42,38]. A summary of the predictions of different theories for the initial conditions immediately after tunnel ionization is given in Table 1.

Using Eqs. (9), (11) and (12), the final momentum of the centre of the distribution in the non-adiabatic regime can be expressed as [38]:

$$\mathbf{P}_{non\text{-}adiab} = C(\gamma)\mathbf{P}_{adiab} \tag{13}$$

where $C(\gamma) = \sinh(\tau_0)/\tau_0$. Since $C(\gamma) > 1$, the non-adiabatic momentum offset is always greater than the corresponding adiabatic expression. The difference between the two is highly sensitive to the Keldysh parameter, γ, which determines τ_0 (see Eq. (8)). For example, for $\gamma = 1$, $C(\gamma) \approx 1.17$, therefore the difference between non-adiabatic and adiabatic cases is relatively small. On the other hand, for $\gamma = 2$, $C(\gamma) \approx 1.45$, meaning that the centre of the momenta distributions are significantly displaced to a higher radius.

Despite significant at higher γ differences in final momenta and exit points between PPT and adiabatic theories, the final angular offset of the centre of the distribution, as obtained from CTMC simulations of Helium, is nearly the same in both models over a wide range of γ. This is because the closer exit point predicted by PPT tends to counter-act the initial non-adiabatic velocity offset such that the ratio of the final momenta along the minor and major axis of polarization, or P_y/P_x, is almost the same whether PPT or TIPIS CTMC simulations are used, at least for ionization of Helium [28]. This good agreement between the PPT and adiabatic models when it comes to the angle of the centre of the momenta distribution is important, since it is precisely from this angle that tunnelling time is extracted with the attoclock method, as will be explained in Section 4.

2.4. Strong field approximation

Strong Field Approximation theory (SFA) can be used to interpret electron momenta distributions at the detector and relate them to physically meaningful events, such as valence electron dynamics inside atoms and molecules. Within SFA, the tunnelling regime holds under *adiabatic* assumptions (corresponding to $\gamma \ll 1$ limit): the bound electron sees an essentially static electric field created by the combined Coulomb and laser fields, and therefore escapes by tunnelling. In this case, the direction of electron emission is determined by the direction of the electric field at the instance of tunnelling. For instance, in the case of linearly polarized light, the electrons are emitted preferentially along the direction of polarization. In contrast, in multi-photon ionization (corresponding to $\gamma \gg 1$) there is no preferred direction of emission, since the electron absorbs

enough photons to go over the top of the potential barrier, following a vertical emission channel. The two ionization channels corresponding to tunnelling and multi-photon ionization are depicted in Fig. 1a.

SFA was originally developed by Keldysh [18], with subsequent seminal developments from Perelomov, and co-authors [42], Reiss [58], and Faisal [59]. Here we present a quick and simple derivation, showing how electron momenta distributions at the detector can be obtained from SFA using saddle point approximation, and how the ADK probability distribution, discussed in the last sub-section emerges in the $\gamma \ll 1$ limit. In principle, all of the results of the previous sub-section that neglect the Coulomb force after ionization and much more [38,58] can be recovered from SFA. For a more detailed treatment, see excellent reviews in [27,43].

We first partition the total Hamiltonian into two parts: $\hat{H} = \hat{H}_0 + \hat{V}$, where $\hat{H}_0$ and $\hat{V}$ are atomic and laser potentials, respectively. In this case, the solution of the time-dependent Schrödinger equation projected onto the velocity basis is given by [27]:

$$\langle \mathbf{v}|\Psi(t)\rangle = -i\int_{t_i}^{t} dt' \langle \mathbf{v}|[e^{-i\int_{t'}^{t}\hat{H}(t'')dt''}]\hat{V}(t')[e^{-i\int_{t_i}^{t'}\hat{H}_0 dt''}]|\Phi_i\rangle \tag{14}$$

where $|\Phi_i\rangle$ is the initial ground state of the atom and is therefore an eigenstate of $\hat{H}_0$, allowing the $\hat{H}_0$ term to be replaced by the ground-state energy, $-I_p$, in Eq. (14). The eigenstates $|\mathbf{v}\rangle$ correspond to the final electron momenta measured at the detector. Therefore, the quantity $|\langle \mathbf{v}|\Psi\rangle|^2$ will give us the density of experimentally measured electron momenta distributions, such as the ones shown in Fig. 1b.

Eq. (14) is known at the time-reversed S-matrix amplitude, and is rather difficult to compute. The crucial simplification of SFA is to neglect the Coulomb force in the term $\hat{H}(t'')$, approximating it instead by the Hamiltonian $\hat{H}_F$ in Eq. (10). This substitution amounts to neglecting the Coulomb field after ionization because it is much weaker than the strong laser field: hence the name Strong Field Approximation. With this substitution, the propagator $e^{-i\int_{t'}^{t}\hat{H}_F(t'')dt''}$ is called the Volkov propagator and the states $\langle \mathbf{v}|$ are Volkov states. It therefore propagates these states backwards in time, from $\langle \mathbf{v}|$ at time t to $\langle \mathbf{v}'|$ at time t'. Eq. (14) now simplifies to:

$$\langle \mathbf{v}|\Psi(t)\rangle = -i\int_{t_i}^{t} dt' e^{-iS(t,t')}\langle \mathbf{v}'|V(t')|\Phi_i\rangle \tag{15}$$

where

$$S(t,t') = \frac{1}{2}\int_{t'}^{t}\left(\mathbf{P} + \mathbf{A}(t'')\right)^2 dt'' - I_p t'. \tag{16}$$

Eq. (15) can be evaluated using a saddle-point method. In particular, the exponent in Eq. (15) is large, $S(t,t') \gg 1$, leading to fast oscillations that largely cancel out, with the most significant contribution at a point, t_s', where t_s' solves $\partial S(t,t')/\partial t' = 0$. Therefore Eq. (15) can be approximated as:

$$\langle \mathbf{v}|\Psi(t)\rangle \propto e^{-iS(t,t_s')}. \tag{17}$$

To find t_s', we take a derivative of Eq. (16) with respect to t' and set it equal to zero, resulting in,

$$\frac{1}{2}\left(\mathbf{P} + \mathbf{A}(t_s')\right)^2 + I_p = 0. \tag{18}$$

For simplicity, let us take linearly polarized light, with polarization along the x-axis, and use a plane-wave vector potential: $\mathbf{A}(t) = (F_0/\omega)\sin(\omega t)\,\hat{x}$, so that $t = 0$ corresponds to maximum electric field pointing along the $-x$-axis. Since we are calculating ionization probability near the peak, the pulse envelope does not play a significant role here. Eq. (18) can now be written as:

$$\frac{1}{2}\left(P_x + \frac{F_0}{\omega}\sin\left(\omega t_s'\right)\right)^2 + \left(I_p + \frac{v_\perp^2}{2}\right) = 0. \tag{19}$$

To determine P_x, we use Eq. (9), substituting $v_x(t_0) = 0$, since velocity along the direction of ionization is zero at tunnel exit, resulting in

$$P_x = -\frac{F_0}{\omega}\sin(\omega t_0) \tag{20}$$

where, as before, t_0 is the instance the electron appears at the tunnel exit. It is clear from the above equation that the momentum at the detector *along the major axis of polarization* is determined solely by the time of ionization. In particular, electrons ionized exactly at the peak of the laser field, end up with $P_x = 0$ at the detector, while the electrons ionized before (after) the peak, corresponding to $t_0 < 0$ ($t_0 > 0$), are accelerated (decelerated) by the laser field relative to $P_x = 0$ electrons and end up with $P_x > 0$ ($P_x < 0$) at the detector. Fig. 4 illustrates experimentally measured momenta distributions for

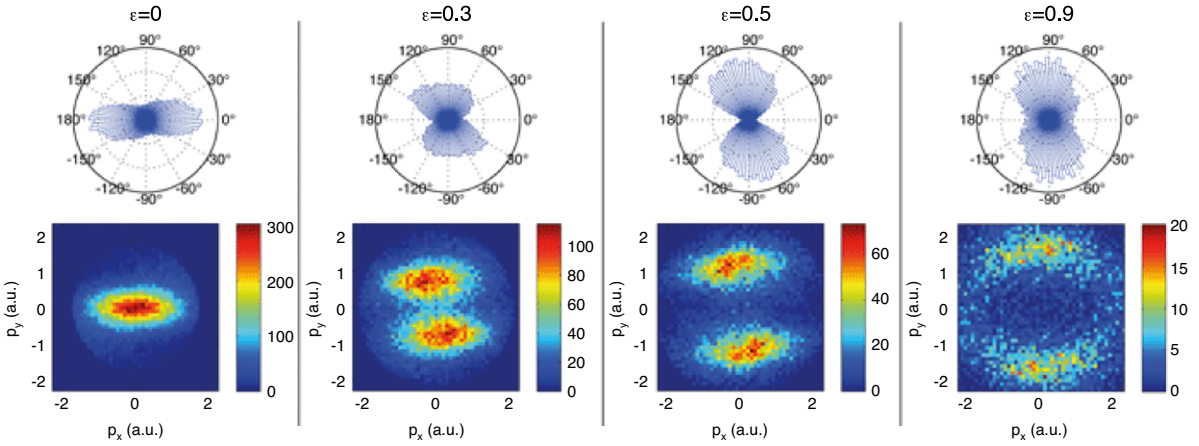

Fig. 4. Experimentally measured electron momenta distributions after strong field ionization for different values of ellipticity, ϵ, of laser light. Peak laser intensity: 8×10^{14} W cm^{-2}, pulse duration (FWHM) of 33 fs, central wavelength of 788 nm.
Source: Taken from [36].

linearly polarized light, or $\epsilon = 0$ (left panel). It is clear that the biggest electron density corresponds to $P_x = P_y = 0$, or to ionization at the peak of the laser field with zero transverse momentum at the tunnel exit.

To calculate probability of ionization at the peak, we substitute $P_x = 0$ into Eq. (19), multiply both sides by $2\,(\omega/F_0)^2$, and use the definition of γ in Eq. (1), resulting in

$$\sin\left(\omega t_s'\right) = \pm i\gamma\left(1 + \frac{v_\perp^2}{2I_p}\right)^{1/2}. \tag{21}$$

In the adiabatic limit, or for $\gamma \ll 1$, $|\omega t_s'| \ll 1$, and t_s' can be approximated as

$$t_s' \approx i\frac{\gamma}{\omega}\left(1 + \frac{v_\perp^2}{4I_p}\right) \tag{22}$$

where a further approximation $v_\perp^2 \ll 2I_p$ and a Taylor expansion of the square-root term in Eq. (21) was used. Only a positive solution was retained in Eq. (22), corresponding (as shall be seen shortly) to a decay of the wave function under the potential barrier. This is indeed the essence of WKB approximation, where only a single decaying solution is taken inside the barrier. Substituting Eq. (22) into Eq. (17), using Eq. (16) with $\mathbf{P} = 0$ and integrating we get after a bit of algebra the ADK probability distribution, given in Eq. (2).

Two points are worthy of note about ionization probabilities derived from SFA. First, the first exponential term in Eq. (2) corresponds to the probability of tunnelling through a static triangular barrier of height I_p and width I_p/F [60]. Hence, in the $\gamma \ll 1$ limit, SFA does indeed reduce to tunnelling through a static short-range (by short-range we mean no Coulomb tail inside the barrier) potential. Second, the other exponential term acts like a momentum filter, preferentially filtering out components with small velocities perpendicular to the direction of tunnelling. This can be understood by considering that the total energy of the bound electron is conserved, so any energy that is expended on transverse motion is lost in the direction of tunnelling, resulting in an effectively wider potential barrier than I_p/F. In fact, as can be seen from Eq. (19), the effective ionization potential corresponds to: $I_p + v_\perp^2/2$.

Importantly, for $v_\perp = 0$, $|t_s'|$ is equivalent to Keldysh time, given by Eq. (24). Since t_s' in Eq. (22) is imaginary, it is often said that Keldysh time is "imaginary" and therefore does not correspond to tunnelling time. This is also sometimes used, in the context of strong field ionization, as an argument for instantaneous tunnelling time, where the time spend under the barrier is "imaginary" with the "real" clock beginning to tick when the electron emerges at the tunnel exit. However, this argument of tunnelling in imaginary time applies equally well to other tunnelling problems, whenever WKB approximation is used (see Eq. (26) and the discussion that follows it). Therefore, it is not yet clear what the connection is between Keldysh time and what is normally meant by tunnelling time. We will come back to this question in Section 2.6 and in the following sections.

2.5. Coulomb effects

As mentioned in the prior sub-section, SFA neglects the Coulomb potential after ionization, predicting electron momenta distributions displaced along the minor axis of polarization only, as given in Eqs. (11) and (13). However, it is clear from Fig. 4 that a small displacement of the centre of the momenta distributions along the x-axis is present as well. This is due to the pull of the parent ion after the electron appears at the tunnel exit. Since most of the Coulomb correction is incurred in

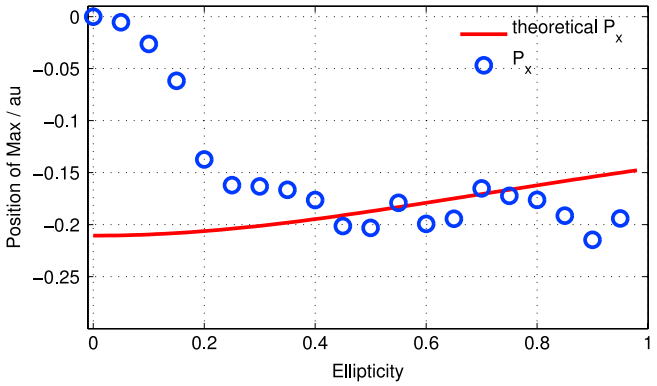

Fig. 5. Experimental values of P_x compared with the perturbative calculation (red curve), given by Eq. (20), following the approach in [41]. All laser parameters are the same as in Fig. 4.
Source: Taken from [47].

the vicinity of the atom, the change in momentum is predominantly along the direction of ionization. Hence the Coulomb correction shifts the centre of the electron momenta distribution predominantly along the x-axis. This imprint of the long-range ionic potential can be seen especially clearly in Fig. 1b, where $p_{x,final}$ and $p_{y,final}$ label the location of the centre of the momenta distribution along the major and minor axes of polarization, respectively. Although SFA predicts $p_{x,final} = 0$, small but significant $p_{x,final}$ is actually observed.

To estimate this additional correction to the final momentum, a perturbative approach has been proposed that freezes the electric field at the instance the electron appears at the tunnel exit [41]. This approach works surprisingly well at higher values of ϵ, as can be seen in Fig. 5. The theoretical curve plotted in Fig. 5 was obtained by using the results obtained in [41] with the exit point taken from TIPIS [26]. In particular, substituting Eq. (6) into $\triangle P_x \approx -(\pi/4)\sqrt{2/F_{max}}x_e^{-3/2}$, given in [41], we obtain:

$$P_x = \triangle P_x \approx -\frac{\pi F_{max}}{\left(I_p + \sqrt{I_p^2 - 4\beta F_{max}}\right)^{3/2}} \tag{23}$$

where $\beta = 1-\sqrt{2I_p}/2$. The analytical estimate given by Eq. (23) breaks down at low values of ϵ. This is somewhat surprising because the perturbative approach is supposed to provide a lower estimate on $|P_x|$, yet Fig. 5 shows that it substantially over-estimates the Coulomb correction for $\epsilon < 0.2$. This has been explained by considering that a significant fraction of low-energy electrons are captured into Rydberg states at low values of ϵ [47]. Hence electrons observed at the centre of the distribution for $\epsilon < 0.2$ actually correspond to electrons ionized before the peak of the E-field. This is yet another modification to the SFA picture and Eq. (2), where the highest electron counts at the detector correspond to maximum field strength, F, and hence electrons ionized at the peak.

In addition to over-estimating P_x, the perturbative approach significantly under-estimates the impact of the long-range potential on P_y for low values of ϵ. In particular, this approach predicts the correction to the momentum to be entirely along the direction of ionization, and hence along the x-axis for ionization at the peak. This is clearly violated for $\epsilon < 0.2$, as can be seen in Fig. 6, where the experimental data for P_y deviates significantly from the Coulomb-free prediction given by Eq. (11) (green curve).

However, as Fig. 6 shows, for higher values of ϵ, where the attoclock operates (see Section 4), there is an excellent agreement between the theoretical prediction that neglects long-range potential and experimentally measured P_y. Likewise, the perturbative estimate for P_x, given by Eq. (23) works well at high ϵ. More precise estimates of corrections due to the force of the parent ion both for P_x and P_y can be performed by running CTMC simulations, as was described in Section 2.2.

To conclude, the effects of the parent ion on the departing electron is important since it rotates the electron momenta distribution (see Fig. 4) increasing the angle from which tunnelling time is extracted with the attoclock method. However, these effects are well-understood and hence the extra angle due to the Coulomb correction can be subtracted from the measurement to get tunnelling time. More details on this method will be given in Section 4.

2.6. Times commonly arising in strong field ionization

By far, the most common time arising in the context of strong field ionization is the Keldysh time. Here, we show the simple procedure of how Keldysh originally calculated what has come to be known as Keldysh time in [18] and relate it to the well-known Büttiker–Landauer time [19]. We also consider the physical arguments for why these times have been suggested as tunnelling time. We want to emphasize that the two times are very closely related and that the validity of one for tunnelling time would immediately imply the validity of the other.

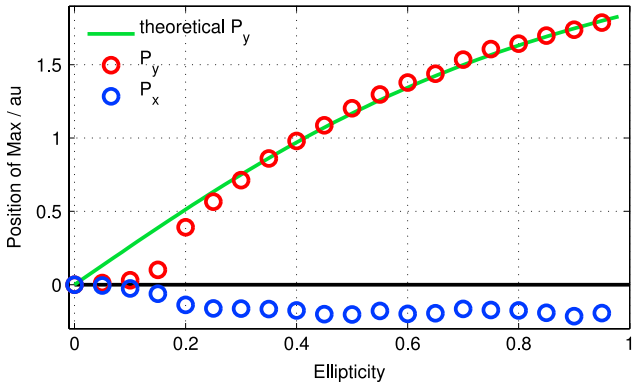

Fig. 6. Centre of the electron momenta distributions P_x and P_y along the major and minor axes of polarization, respectively, obtained from experiment. Theoretical curves correspond to expected values in the absence of any Coulomb interaction for P_y (green curve) and P_x (horizontal black line). Experimental P_x data points are the same as in Fig. 5.
Source: Taken from [47].

Table 2
Commonly used definitions of tunnelling times. Each one depends on the transmission amplitude, T, of the wave function through the potential barrier.

Name	Type	Symbol	Definition
Büttiker–Landauer	Probability-dependent	τ_{BL}	$-\hbar\partial ln\|T\|/\partial V$
Pollack–Miller	Probability-dependent	τ_{PM}	$\hbar\partial ln\|T\|/\partial E$
Eisenbud–Wigner	Phase-dependent	τ_{EW}	$\hbar\partial\theta/\partial E$
Larmor	Phase-dependent	τ_{LM}	$-\hbar\partial\theta/\partial V$

The Keldysh time was obtained by calculating the classical time it would take for a point particle to travel through the inverted triangular barrier [18]. In particular, the kinetic energy of the electron was taken to be equal to the ionization potential: $KE = (1/2)\ mv^2 = I_p$, resulting in $v = \sqrt{2I_p}$, where Keldysh [18] dropped the mass of the electron, since it is equal to one in atomic units. (That I_p is indeed the average kinetic energy of the bound electron easily follows from the virial theorem for $1/r$ potential: $2KE = -PE$, where KE and PE are average kinetic and potential energies, respectively.) Calculating the time it would take to decelerate an electron from velocity $v = \sqrt{2I_p}$ to zero (the barrier exit point) while applying a constant deceleration of F, which is the strength of the electric field, we get Keldysh time:

$$\tau_K = \sqrt{2I_p}/F. \tag{24}$$

Therefore it seems clear that Keldysh was viewing τ_K as the physical amount of time it would take the electron to cross the distance of a barrier, I_p/F, while being decelerated by an electric field of the laser. The physical justification to assigning the meaning of tunnelling time to this classical calculation arises when considering the non-adiabaticity parameter, γ, which can be rewritten as:

$$\gamma = \omega\tau_K. \tag{25}$$

From this equation, it is clear that if the tunnelling time, τ_K, is long, compared to the frequency of the laser field, then $\gamma \gg 1$, and the electron sees a quickly oscillating laser field and absorbs many photons, going over the barrier (vertical channel in Fig. 1a). On the other hand, if the tunnelling time, τ_K, is fast compared to ω than the electron sees a static field while tunnelling and the problem is essentially adiabatic. Hence, the physical justification for viewing τ_K as the tunnelling time is based on explaining the transition to non-adiabatic tunnelling as arising from the barrier transversal time becoming comparable in magnitude to the time-variation of the potential barrier.

This was precisely the physical motivation behind the Büttiker–Landauer time [19]: a more general definition which reduces to the Keldysh time when applied to tunnelling through a triangular barrier of width I_p/F. Within the WKB approximation, this definition is equivalent to [19]:

$$\tau_{BL} = \int_{x_0}^{x_e} \frac{m}{p(x)}dx = \int_{x_0}^{x_e} \frac{\sqrt{m/2}}{(V(x)-E)^{1/2}}dx \tag{26}$$

where x_0 and x_e are entrance and exit points from the barrier, respectively, m is the mass, and the (imaginary) momentum is given by: $p(x) = \sqrt{2m\,(V(x)-E)}$. An alternative definition of the Büttiker–Landauer time (equivalent within the WKB approximation) will be given in the following section (see also Table 2).

The integral in Eq. (26) is real, since $V(x) > E$ everywhere inside the potential barrier. However, it is clear that Eq. (26) would give imaginary time, if the momentum $p(x)$ was defined the usual way. Hence, τ_{BL} is imaginary in the same way that the Keldysh time was shown to be imaginary in Section 2.4. This property simply follows from $V(x) > E$ inside the forbidden region, resulting in imaginary momentum and, since the width of the barrier is real, traversal in imaginary time.

In spite of τ_{BL} becoming imaginary when the "proper" definition of momentum is inserted into Eq. (26), Büttiker and Landauer argued that it must be the actual barrier transversal time because it determines the onset of the 'cross-over' regime between pure tunnelling and tunnelling while absorbing one or more photons from the oscillating field [19]. In particular, Büttiker and Landauer used a rectangular barrier of height V_0 with a low amplitude oscillation of magnitude $V_1 \ll V_0$ and frequency ω_b. They found that for $\omega_b \tau_{BL} \sim 1$, the tunnelled electron was likely to have absorbed a photon, suggesting that the electron "knew" about the time-dependent oscillation in the field while tunnelling. This, in turn, was interpreted as suggesting that the time-scale of the tunnelling process was comparable to the time-scale of the oscillation. Hence $\omega_b \tau_{BL}$ is similar to the Keldysh γ in separating adiabatic tunnelling from the regime where quanta of energy are absorbed from the oscillating field. Despite some theoretical problems in interpreting τ_{BL} as tunnelling time apparent in the limit of thin barriers [14], the physical interpretation sketched out above was appealing and the Büttiker–Landauer time remained a very popular contender for tunnelling time in the last few decades. We will compare it with the attoclock measurements in Section 4.

Recently, it has been found that Keldysh time (and hence, as we have explained above, the Büttiker–Landauer time) is proportional to the time it takes the system to reach static ionization rates after a sudden turn-on of the potential [23]. In this case, contrary to the suggestion in [23], Keldysh time would not actually correspond to tunnelling time, as it is typically defined. Note that the Büttiker–Landauer time is actually well-defined for static potentials, and is referred to by Büttiker and Landauer as a "time a tunnelling particle interacts with its barrier" or the "barrier traversal time". The results in [23] are nevertheless relevant since they suggest that both the Keldysh and the Büttiker–Landauer times may be more representative of the transient behaviour of wave functions in time-dependent potentials, rather than as a practically useful definition of tunnelling time. The relationship between the Keldysh time and this transient behaviour, however is still far from clear, since the proportionality constant between the two times was found numerically in [23] to depend on a particular shape of the potential, but without physical or mathematical justification as to why different potentials resulted in different constants, or what these constants should be on theoretical grounds.

Another time, called Eisenbud–Wigner (or Wigner–Smith) time [61], has been widely used to calculate time delays in single photon ionization with attosecond pulses [10,62–66]. As mentioned in Section 3.1, this time is more problematic for tunnelling, since the peak of the wave-packet in this case is not well-defined. In addition, it is not clear how to define the Eisenbud–Wigner time for tunnel ionization, since the Hamiltonian in this case is time-dependent due to the strong laser field, in contrast to assumptions used to derive the Eisenbud–Wigner time in [61]. In particular, this time was derived for static potentials which asymptotically go to zero for large distances, with the relative Eisenbud–Wigner time being determined by the phase difference between near-monochromatic wave packets of the same energy propagating in a vacuum and in a potential, respectively. Hence, this time is well-suited to study single photon ionization, where an attosecond pulse is assumed to instantaneously promote the electron into a continuum, at which point it interacts only with the time-independent potential of the parent ion. However, this set of assumptions is *not* satisfied in tunnel ionization, where the dominant terms in the Hamiltonian immediately after tunnel ionization are determined by the time-dependent laser fields. Nevertheless, the Eisenbud–Wigner time can be calculated following the definition given in Table 2, although standard methods of matching the outgoing to the bound-state wave function, such as was done in [67,68], fail in this case since phase information is lost, incorrectly predicting instantaneous tunnelling for phase times, such as Eisenbud–Wigner and Larmor times (see Section 4.4 for more details) [69].

3. Tunnelling time theory

While tunnelling probabilities, such as the ones presented in the previous section, are well defined and widely accepted, the question of how long it takes a particle to transverse a barrier has been the subject of intense debate for decades. Since MacColl [11], there have been repeated attempts to address this question with "no clear consensus, however, about the existence of a simple expression for this time, and the exact nature of that expression" [12]. To complicate matters, the tunnelling time itself is not well defined. Different definitions exist, arguably related to different and complementary aspects of the tunnelling problem and depending on the experimental context.

Here, we will start with the four commonly used definitions of tunnelling time (Section 3.1), followed by a Feynman path integral (FPI) approach that can be used to calculate probability distribution of tunnelling times in Section 3.2. We then show in Section 3.3 that within the FPI formulation, the common tunnelling time definitions can be viewed as averaged quantities, rather than deterministic values. We also indicate the connection between the FPI approach and the increasingly influential in quantum mechanics theory of weak measurement [70]. The theory presented here will be compared with the attoclock measurements in the context of strong field ionization in Section 4.

We want to emphasize that the theoretical treatments of tunnelling times described here are by no means exhaustive and that other approaches exist, such as Bohmian trajectories [71] or Wigner paths distribution. For more detailed accounts, see for example [12,14].

3.1. Definitions of tunnelling time

There are four widely used definitions of tunnelling time, which can be classified as either "probability dependent" or "phase dependent". Here we will briefly review these four tunnelling times, as well as indicate their relationship to each other, to be discussed again in Section 3.3. The four times are: **Larmor** time [72,73], τ_{LM}, the **Büttiker–Landauer** time [19], τ_{BL}, the **Eisenbud–Wigner** time [61], τ_{EW}, and the **Pollack–Miller** time [74], τ_{PM}. All of these times are based on very different models, but they can all be expressed in terms of the transmission amplitude: $T = |T|e^{i\theta}$, the height of the potential, V, and the incident energy of the particle, E. The first two times depend on the potential and have been called the *resident (or dwell) time* [75],

$$\tau_{BL} = -\hbar\partial ln|T|/\partial V; \qquad \tau_{LM} = -\hbar\partial\theta/\partial V. \tag{27}$$

The other two times depend on the incident energy of the particle and have been called the *passage time*,

$$\tau_{PM} = \hbar\partial ln|T|/\partial E; \qquad \tau_{EW} = \hbar\partial\theta/\partial E. \tag{28}$$

A summary of different definitions and their dependence either on the probability or phase of transmission is given in Table 2.

The correspondence between the two different expressions for τ_{BL}, given by Eqs. (26) and (27) can be shown by solving for $|T|$, to lowest order, using the WKB approximation,

$$|T| \approx Ce^{-\int_{x_0}^{x_e} dx\sqrt{2m(V(x)-E)}} \tag{29}$$

where C is a constant and substituting Eq. (29) into Eq. (27), which will result in Eq. (26).

Note that in Eq. (27) the derivative with respect to V means a variation of δV everywhere inside the potential barrier, as shown in Eq. (30). In particular, it means that when applying these times to strong field ionization, the derivative ∂V cannot be replaced with ∂I_p, unless $\partial V/\partial I_p = 1$ everywhere inside the potential barrier. This is in general not true whenever the Coulomb potential inside the barrier is included, in which case, $V(x)$ becomes a nonlinear function of I_p, where x is taken to be the direction of tunnelling (for example, see the potential along the tunnelling coordinate of a fully-solvable problem of a Hydrogen atom in a static electric field [57]).

The two times in Eq. (27) were elegantly combined by Sokolovski and Baskin [76] into a single complex time, given by:

$$\tau_T^{\Omega} = \tau_{LM} - i\tau_{BL} = i\hbar\int_{\Omega} dx\frac{\delta\, lnT}{\delta V(x)} \tag{30}$$

where Ω denotes the barrier region (for an experiment which attempts to measure both components of the complex time, see [77]). The subscript T denotes that the time spent inside the barrier is for transmitted particles, with a similar expression, τ_R^{Ω}, developed for reflected particles [76],

$$\tau_R^{\Omega} = \tau_{LM}^R - i\tau_{BL}^R = i\hbar\int_{\Omega} dx\frac{\delta\, lnR}{\delta V(x)} \tag{31}$$

where R is the reflection coefficient, and the superscript R denotes particles which eventually get reflected from the potential barrier. By substituting $T = |T|e^{i\theta}$ into Eq. (30), it is easy to verify that $Re\left(\tau_T^{\Omega}\right)$ and $-Im\left(\tau_T^{\Omega}\right)$ correspond to the Larmor time and the Büttiker–Landauer time, respectively, as given in Eq. (27).

The Larmor clock for measuring tunnelling time was originally proposed by Baz' [72] and Rybachenko [73]. The idea is to use spin polarized electrons and a potential barrier with a constant magnetic field inside, as shown in Fig. 7. In this case, the time spend inside the barrier, or τ_{LM}, is given by the degree of precession of the electron spin: $\tau_{LM} = \theta_y/\omega_L$, or in terms of the averaged spin component $\langle s_y\rangle$ [14],

$$\tau_{LM} = \tau_y = \lim_{\omega_L\to 0}\langle s_y\rangle/\left(-\frac{1}{2}\hbar\omega_L\right) \tag{32}$$

where ω_L is the Larmor frequency given by: $\omega_L = (e/2m_e)\,B$, and the angle, θ_y corresponds to the degree of rotation of the spin in the x–y plane. Here, the limit of infinitesimal magnetic field is taken, reflected by $\omega_L \to 0$, so that only the first order effects need to be retained in the expression. A generalization of the Larmor time to arbitrary potential barriers was proposed by Leavens and Aers [78,79], and is given by τ_{LM} in Eq. (27).

However, it was pointed out by Büttiker [80] that the depiction in Fig. 7 of Larmor clock is not accurate, since the barrier preferentially transmits spin up states. In particular, an electron spin polarized along the x axis can be expressed as an equal combination of spin up and spin down states along the z axis. Since the spin states aligned with the magnetic field are lower in energy, the effective potential barrier is lowered and such states are preferentially transmitted. In particular, the transmission probability of spin up $(+)$ and spin down $(-)$ states, where spin is aligned along the z-axis, are given by:

$$T_{\pm} = Te^{\pm\omega_L\tau_z} \tag{33}$$

where T is the transmission amplitude in the absence of spin, and τ_z is the "new" Larmor clock component corresponding to the rotation in the x–z plane, and given by

$$\tau_z = \lim_{\omega_L\to 0}\langle s_z\rangle/\left(-\frac{1}{2}\hbar\omega_L\right) \tag{34}$$

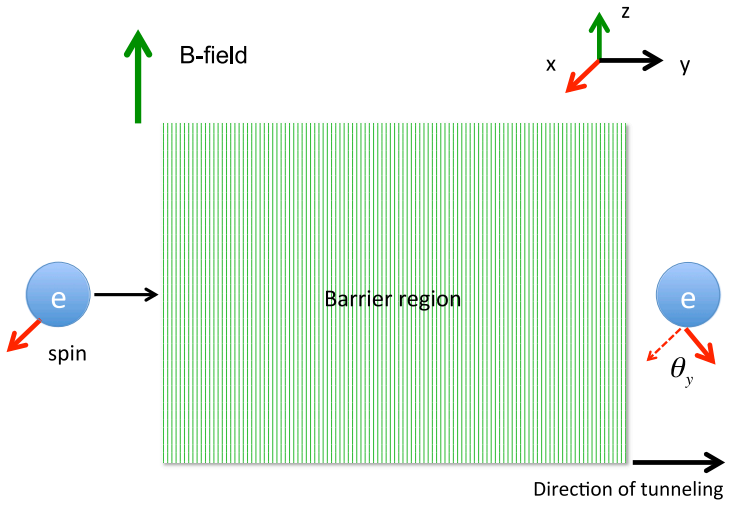

Fig. 7. Larmor clock proposed by Baz' [72] and Rybachenko [73]. Spin polarized electrons, with spin s_x, enter a potential barrier where a constant magnetic field points along the z-axis. When the electron exits the potential barrier, it acquires an additional spin component along the y-axis due to Larmor precession inside the barrier. The precession angle of the spin determines the amount of time the electron spends inside the barrier.

where $\langle s_z \rangle$ is the average spin component acquired by the transmitted electrons along the z-axis. Because the transmission probability scales exponentially with effective barrier height, this results in a substantial rotation of the transmitted spin in the y–z plane, to align with the B-field, such that: $\langle s_z \rangle \gg \langle s_y \rangle$, resulting in $\tau_z \gg \tau_y$.

Büttiker showed that τ_{BL} is equal to τ_z, and for deep potential barriers can be approximated as

$$\tau_{BL} = \sqrt{\tau_y^2 + \tau_z^2} = |\tau_T^{\Omega}|. \tag{35}$$

The physical justification behind τ_{BL} giving the duration of the tunnelling process was already given in Section 2.6. In short, it was due to the fact that τ_{BL} can be used to determine the 'cross-over' regime between adiabatic tunnelling and tunnelling while exchanging energy with the oscillating potential barrier [19]. It was pointed out in [14] that this justification is not in general valid with an example of an infinitely thin, but high barrier: $d \to 0, V_0 \to \infty, V_1 \to \infty$, where τ_{BL} vanishes, but the 'cross-over' regimes still exists, showing that these two concepts are qualitatively different, although they coincide in the case of opaque barriers [14]. Additional justification for using τ_{BL} to time the duration of tunnelling was provided by Büttiker in [80] by retrieving τ_{BL} from Larmor clock times, τ_y and τ_z, as explained above (see Eq. (35)).

It is argued in [14], that a necessary requirement for a physically meaningful tunnelling time, τ_T, is that it satisfies the relation,

$$\tau_{dwell} = |R|^2 \tau_R + |T|^2 \tau_T \tag{36}$$

where τ_{dwell} is the dwell time inside the potential barrier (see Eq. (38)), which includes both reflected and transmitted components, R and T are reflection and transmission coefficients, respectively, and τ_R and τ_T are the associated times. It was shown that the Larmor time satisfies this condition, while the Büttiker–Landauer time does not [76]. This easily follows from the following relationship proven by Sokolovski and Baskin [76],

$$\tau_{dwell} = |R|^2 \tau_R^{\Omega} + |T|^2 \tau_T^{\Omega} \tag{37}$$

where τ_T^{Ω} and τ_R^{Ω} are complex valued times given by Eqs. (30) and (31), respectively. Equating real and imaginary components of Eq. (37) and using Eqs. (30) and (31), it follows that the transmitted and reflected Larmor times satisfy Eq. (36), but the corresponding Büttiker–Landauer times do not.

The requirement for physically meaningful tunnelling time to satisfy Eq. (36) is compelling because τ_{dwell} denotes the total time spent by a particle inside the barrier, whether it was eventually transmitted or reflected. It is given by a simple expression, originally introduced by Smith [82] which divides the total particle density inside the barrier by the incoming group velocity, $v(k) = \hbar^{-1}\, dE/dk$,

$$\tau_{dwell} = \frac{1}{v(k)} \int_{x_0}^{x_e} dx |.\Psi\ (x; k)\ |^2. \tag{38}$$

Since $|R|^2$ and $|T|^2$ correspond to reflection and transmission probabilities, respectively, Eq. (36) corresponds to the requirement for the total time spend inside the barrier to be equal to the weighted sum of transmitted and reflected times.

The Eisenbud–Wigner phase time, or τ_{EW} defined in Eq. (28), follows the peak of the propagating wave-packet [61], calculating the *additional* phase-shift acquired by the wave-packet due to the interaction with a time-independent potential.

Therefore, it is important to keep in mind that τ_{EW} is not the total delay time, but an additional delay due to the presence of a potential. For instance, in propagation through a potential barrier of width w for a particle with incoming velocity $\hbar k$, the total barrier traversal phase time is given by:

$$\tau_{tot} = \frac{w}{\hbar k} + \tau_{EW}. \tag{39}$$

The E–W time was derived by considering a nearly mono-chromatic wave packet, propagating with velocity $v = \hbar k/m$, in a continuum state interacting with a spherical potential [61]. It was shown that such a wave-packet is retarded by a distance $\triangle d = 2\partial\theta/\partial k$, resulting in a time shift given by:

$$\triangle t = 2\tau_{EW} = \frac{\triangle d}{v} = 2\hbar\frac{\partial\theta}{\partial E} \tag{40}$$

where we used the chain rule and $E = \hbar^2 k^2/2m$. In the above equation, the τ_{EW} is multiplied by a factor of 2. This is due to the fact that the time shift is accumulated both when the wave packet is moving toward the potential and when it is moving away from it. Hence, in ionization experiments, where the wave packet only moves away from the parent atom, only half of the time-shift is incurred.

While the application of E–W time is relatively straight-forward when the energy of the wave packet is above that of the potential: $E > V(r)$, it is much more problematic when tunnelling is involved. In particular, no peak of the wave packet exists inside the barrier for a tunnelling particle [14] and a large part of the wavefunction remains confined. For non-monochromatic wave packets, the barrier filters out the higher energy components [83,84], resulting in negative phase delay times [12].

Hence, the E–W time is best suited to the near-monochromatic electron wavepacket that is already promoted into the continuum, such as after absorbing one or more photons in ionization experiments. It was therefore used extensively to explain the relative time delays in single photon ionization [10,62–66], where the momentum of the electron is well defined and the energy is above the ionization threshold. In principle, E–W time can just as easily be applied to multi-photon ionization, as long as no tunnelling is involved. However, since ionization with the strong IR field typically involves tunnelling, or some mix of tunnelling and multi-photon ionization components (see Section 2.2), the E–W time may not be the most appropriate, although the definition given by Eq. (28) can still be applied.

The Pollack–Miller time [74] was calculated by using flux–flux correlation functions, commonly used in chemical kinetics. With this definition, the time of the collision is defined as the average correlation time. Although the Pollack–Miller and the Eisenbud–Wigner times were derived using very different physical models, they can be combined in the same way as the Larmor and the Büttiker–Landauer times were combined into a single complex time in Eq. (30),

$$\tau_{EW,PM} = \tau_{EW} - i\tau_{PM} = -i\hbar\frac{\partial lnT}{\partial E}. \tag{41}$$

All four times in Eqs. (27) and (28) can be derived in a unified manner using Gell-Mann–Hartle decoherence functionals [81] combined with a Feynman path integral approach [75]. We will show in Section 3.3 how within the Feynman path integral approach these four times naturally arise as averaged quantities, rather than deterministic values.

3.2. Feynman path integral formulation for tunnelling time

Feynman path integral approach has proven to be very fruitful not only in quantum mechanics, but in stochastic systems [85], and has even found an interesting application in noise-induced escape due to a far from equilibrium fluctuation [86]. When it comes to tunnelling time, it has the advantage of expressing the total wavefunction $\Psi(x, T)$ as a sum over all "possible" paths (see Fig. 8), with each path contributing $exp[iS[x_j(t)]]$, where $S[x_j(t)]$ is the action for a particular path $x_j(t)$ with endpoints: $x_j(0) = x'$ and $x_j(T) = x$,

$$S[x_j(t)] = \int_0^T [\left(m\dot{x}_j\right)^2/2m - V(x_j)]dt. \tag{42}$$

The total wavefunction is then given by [85],

$$\Psi(x, T) = \int dx' \int Dx_j(t) exp[iS[x_j(t)]/\hbar]\Psi\left(x', 0\right). \tag{43}$$

Since each path is deterministic, it is possible to associate to each $x_j(t)$ a time that it spends inside the barrier region. The idea is then to separate the paths that spend an exact amount of time τ inside of the barrier, resulting in a wavefunction composed only of these paths,

$$\Psi(x, T|\tau) = \int dx' \int Dx_j(t)\delta\left(t_b[x_j(t)] - \tau\right)\exp\left(iS[x_j(t)]/\hbar\right)\Psi\left(x', 0\right) \tag{44}$$

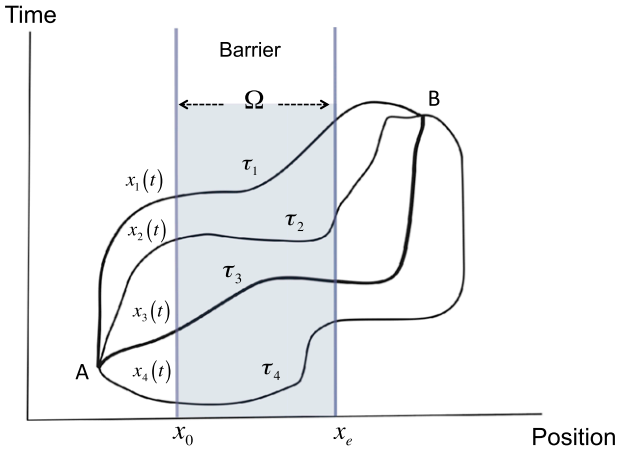

Fig. 8. The propagator corresponds to the sum of the all possible paths between points A and B, each path, $x_j(t)$ contributing $e^{iS[x_j(t)]}$, where S is defined by Eq. (42).

where $t_b[x_j(t)]$ is the time spend inside of the barrier region by $x_j(t)$. Note that the barrier transversal time here is well-defined since $x_j(t)$ is deterministic, with t_b given by [87,88],

$$t_b[x(t)] = \int_0^T \Theta(x(t))dt \tag{45}$$

where $\Theta(x(t)) = 1$ for $x_0 \leq x(t) \leq x_e$, and is equal to zero otherwise. Here, x_0 and x_e are the entrance and the exit points of the tunnel, respectively. Eq. (45) gives the resident (dwell) time or the time a particle spends inside the barrier region.

It has been shown that the wavefunction in Eq. (44) satisfies the following "clocked" Schrödinger equation [88],

$$i\hbar\frac{\partial\Psi\,(x,\,t|\tau)}{\partial t} = -\frac{\hbar^2}{2m}\frac{\partial^2\Psi\,(x,\,t|\tau)}{\partial x^2} + V(x)\Psi\,(x,\,t|\tau) - i\hbar\Theta(x)\frac{\partial\Psi\,(x,\,t|\tau)}{\partial\tau}. \tag{46}$$

From Eq. (44), it is clear that the total wavefunction can be expressed as an integral sum of the $\Psi\,(x,\,T|\tau)$ wavefunctions,

$$\Psi\,(x,\,T) = \int_0^\infty \Psi\,(x,\,T|\tau)\,d\tau. \tag{47}$$

Therefore, the total wavefunction is the sum of the interfering wavefunctions that correspond to the amount τ that the particle spends traversing a barrier, much like the interference pattern in a double-slit experiment is composed of wavefunctions going through each slit.

The relation in Eq. (44) has been expressed in propagator form as [87,89],

$$G_\tau\,(k_0, x_e, x_0) = t\,(k_0, V|\tau)\,G_0\,(k_0, x_e, x_0) = \int_{-\infty}^{\infty} dt e^{iE_0 t/\hbar}\int_{x(0)=x_0}^{x(T)=x_e} Dx_j(t)\delta\left(t_b[x_j(t)] - \tau\right)e^{iS[x_j(t)]/\hbar} \tag{48}$$

where $t\,(k_0, V|\tau)$ is the contribution of paths spending time τ inside the barrier to the transmission amplitude $t(k_0, V)$ [89], and $G_0\,(k_0, x_e, x_0)$ is the propagator in the absence of a barrier. The total transmission amplitude is given by: $t\,(k_0, V) = \int_{-\infty}^{\infty} t\,(k_0, V|\tau)\,d\tau$.

The δ function in Eqs. (44) and (48) can be written in the following form:

$$\delta(t_b(x_j) - \tau) = \frac{1}{2\pi\hbar}\int_{-\infty}^{\infty} dW\, exp^{-iW[(t_b(x_j)-\tau)/\hbar]}. \tag{49}$$

Substituting Eq. (49) into Eq. (48) and using Eqs. (42) and (45), we see that each term in Eq. (49) is equivalent to adding a rectangular potential of height $W\Theta(x)$ to $V(x)$. If we denote the transmission amplitude in the presence of the potential $W\Theta(x) + V(x)$ by $t(k_0, V + W)$, Eq. (48) becomes [87,89]:

$$t(k_0, V|\tau) = \frac{1}{2\pi\hbar}\int_{-\infty}^{\infty} dW\, exp^{iW\tau/\hbar}t(k_0, V + W). \tag{50}$$

Each $t(k_0, T|\tau)$ is a probability amplitude that a particle impinging on a barrier with energy E will spend time τ inside it before being transmitted. *The above equation gives a prescription for calculating the part of the wavefunction that corresponds to a specific time τ that the electron spends inside the potential barrier before being transmitted.*

An alternative definition to the dwell or residence time, given by Eq. (45) is the passage time which corresponds to the difference between the last time a path left the barrier at x_e and the first time it entered at x_0. For the passage time, the amplitude in Eq. (50) is modified to [75]

$$t_p(k_0, V|\tau) = \frac{\hbar k_0}{2\pi m}\int_{-\infty}^{\infty} dk\, exp^{-iE\tau/\hbar} t(k_0 + k, V) \tag{51}$$

where $E = \hbar^2 k^2/2m$. Dwell time amplitude, given by Eq. (50) is more commonly used than the passage time. As shown in Section 3.3, it can be used to obtain Büttiker–Landauer and Larmor times. The residence time was shown to give Pollack–Miller and Eisenbud–Wigner times [75].

Here, we have to quote Landauer: "Now, there is little doubt that the propagator [in Eq. (48)] contains information about paths that traverse the barrier and spend a time τ in the process. But it is not clear what procedure is needed to calculate physical quantities with the Feynman approach" [12]. The problem arises from the fact that histories corresponding to different τ are not mutually exclusive, but rather interfere. A good analogy here is the well-known double (or multiple) slit experiment, that Feynman said lies at "the heart of quantum mechanics" [90]: the probabilities that the electron will go through different slits are not mutually exclusive, but interfere. Formally this means that the wavefunction $\Psi(x, T|\tau)$ does not satisfy the weak decoherence condition [91], given by

$$Re\, D[\tau;\tau'] = \delta\left(\tau - \tau'\right) P(\tau) \tag{52}$$

where $D[\tau;\tau']$ is the decoherence functional [81],

$$D[\tau;\tau'] = \lim_{t\to\infty}\int_{x_e}^{\infty} dx \Psi^*(x, t|\tau)\, \Psi\left(x, t|\tau'\right) \tag{53}$$

thereby preventing the construction of a probability distribution of tunnelling times. However, it is possible to define a range of values of τ [91], such as might be obtained within experimental accuracy. In particular, the prescription for calculating the probability distribution of tunnelling times with the FPI approach requires coarse-graining [87]. Coarse-graining is introduced by the measurement device, as traditionally defined by von Neumann, and is determined by the accuracy of the measurement. In the case of a presence of such measurement device and the resultant coarse-graining, it has been shown in [92], that the weak decoherence condition is indeed satisfied, thereby allowing for the construction of a probability distribution of tunnelling times. The coarse-grained tunnelling time probability amplitude is given by [87],

$$\langle t(k_0, V|\tau)\rangle = \int_0^{\infty} t(k_0, V|\tau') e^{-\left(\tau-\tau'\right)^2/\tau_0^2} d\tau' \tag{54}$$

where τ_0 in Eq. (54) is determined by the measurement. The coarse grained unnormalized probability distribution is then given by $|\langle t(k_0, V|\tau)\rangle|^2$ and depends on the accuracy of the measuring device. Like other definitions of tunnelling time expressed using FPIs (see the following subsection), coarse graining involves integration over τ and therefore resolves the issue of having arbitrarily high frequencies of non-vanishing amplitude contained in $t(k_0, V|\tau)$.

In Section 4, we will show the FPI probability distribution of tunnelling times constructed for strong field tunnel ionization and compare it to the attoclock measurements. In particular, it will be shown that, in agreement with conclusions in [91], the range of possible tunnelling times is quite broad, hence it is hard to speak of a unique tunnelling time. From that viewpoint, it is more appropriate to view the four definitions of tunnelling time introduced in this section as average, rather than deterministic values.

3.3. Tunnelling time definitions expressed as averaged values and weak measurement

Here we show how the four definitions of tunnelling time can be related to each other using the FPI approach, as well as the relation between the complex time that results from the FPI method and the weak measurement theory. The four definitions of tunnelling time presented in Section 3.1 can all be expressed as different averages using the FPI probability amplitudes. To understand how these times relate to the Feynman path integral approach, we define an average tunnelling time as [20]:

$$\tau_T^{\Omega} = \frac{\int_0^{\infty} t(k_0, V|\tau)\tau d\tau}{\int_0^{\infty} t(k_0, V|\tau) d\tau} \tag{55}$$

where the denominator in the above equation is for normalization. The above equation has been shown to be equivalent to τ_T^{Ω} in Eq. (30) [12,20], hence the same label is used. Similarly, the same expression for $\tau_{EW,PM}$ given in Eq. (41) can be obtained by performing the following average [21],

$$\tau_{EW,PM} = \frac{\int_0^{\infty} t_p(k_0, V|\tau)\tau d\tau}{\int_0^{\infty} t_p(k_0, V|\tau) d\tau} \tag{56}$$

where $t_p(k_0, V|\tau)$ is the passage (rather than resident) time amplitude given by Eq. (51).

The expression in Eq. (55) can alternatively be put in the following form,

$$\tau_T^{\Omega} = \frac{\langle \Psi_f | \tau | \Psi_i \rangle}{\langle \Psi_f | \Psi_i \rangle} \tag{57}$$

where Ψ_f and Ψ_i correspond to the transmitted and incident parts of the wavefunction, respectively. The real part of Eq. (57) corresponds to the **weak measurement value** of tunnelling time, [93,94]

$$\tau_{weak} = Re \frac{\langle \Psi_f | \tau | \Psi_i \rangle}{\langle \Psi_f | \Psi_i \rangle} = Re \left(\tau_T^{\Omega} \right). \tag{58}$$

A physical interpretation of the complex expectation value that arises when weak measurement is used was recently suggested in [95]. Earlier, the interpretation of the complex tunnelling time in Eq. (57) was provided in [94], where the real and imaginary parts were proposed to correspond to different properties of the measuring device, represented as a pointer.

From Eqs. (30) and (58), it is clear that the weak measurement value of tunnelling time corresponds to Larmor time [96,94], or

$$\tau_{LM} = \tau_{weak}. \tag{59}$$

An influential idea, first introduced by Aharonov and colleagues [70] in 1988, is to use a measurement that is so weak that it does not significantly perturb the system. This is in contrast to von Neumann type of measurement, which collapses the system into one of its eigenstates (such measurement is known as a strong measurement). While weak measurement does not significantly perturb the system, it also does not provide much information about the state of the particle: imagine a pointer with a very large uncertainty in its position [94]. Although a single weak measurement does not contain much information, a statistical ensemble of such measurements can provide highly accurate information about the system.

By combining many weak measurements, a recent experiment was able to gain some information about the paths taken by photons in a two-slit experiment without destroying the interference pattern [97]. This challenges a widely held notion within conventional quantum mechanics that it is "forbidden" to ask which of the slits a particle has gone through in a two slit experiment (for more detailed discussion, see for example [98]). Another application of weak measurement, experimentally showed that the Heisenberg uncertainty principle can be violated in its original formulation of the "measurement–disturbance relationship" [99]. Steinberg, a group leader in these two experiments [97,99] has previously proposed the answer to the tunnelling time question in terms of the weak measurement, pointing out its close relation to the Larmor time [94].

4. Measurement of tunnelling time with the attoclock

4.1. Prior experiments on tunnelling time

Prior experiments on tunnelling time roughly fall into two categories. The first involves the measurement of electron currents through circuits, while the second extracts tunnelling time from propagation of light.

One notable tunnelling time experiment involved measuring electron current through the Josephson junction [100]. The tunnelling time in this case was found to agree, within an order of magnitude, with the Büttiker–Landauer time [15]. Another experiment measured the propagation of electromagnetic wave packets through 1D photonic band gap materials, finding superluminal tunnelling that was independent of the barrier thickness for opaque barriers [83]. However, since classical wavepackets were used in [83], such superluminal propagation can be understood as a result of a "pulse reshaping process", in which a medium preferentially allows passage of a higher energy components of the wavepacket in such a way that the transmitted peak appears shifted forward in time.

To date only two experiments [9,101] were done at the single particle level, thereby avoiding the possibility of a "pulse reshaping process". The experiment in [101] showed that a *single photon* going through a barrier arrives at the detector faster than the photon covering the same distance in a vacuum. This resulted, of course, in faster than the speed of light propagation through the potential barrier, which was explained by the authors [101] by invoking the theory of weak measurement. The experiment in [101] also compared some of the theories of tunnelling time presented in Section 3.1 to measurements, ruling out the Büttiker–Landauer time as a likely candidate. However, for optimal comparison with theories presented in Section 3, the tunnelling time of a non-relativistic electron (as opposed to a photon), in other words a particle that obeys the Schrödinger equation, is desirable.

The first attoclock experiments were performed in [9] and put an upper limit on a single electron tunnelling delay time of around 40 as. This made tunnelling possibly instantaneous, within experimental error, and also ruled out the Büttiker–Landauer time, which was about an order of magnitude too large. However, the experiment in [9] was performed over a very narrow intensity range, and hence did not observe any trends in tunnelling time, or make a comparison with theories other than the Büttiker–Landauer time. Section 4.2 will give a brief overview of how tunnelling time is extracted from the attoclock measurements, building on concepts first introduced in Section 2. Section 4.3 describes most recent attoclock measurements performed over a much wider intensity range and using two different experimental apparatus (COLTRIMS and VMIS). Section 4.4 discusses how these new measurements compare to the different theoretical definitions of tunnelling time introduced in Section 3.

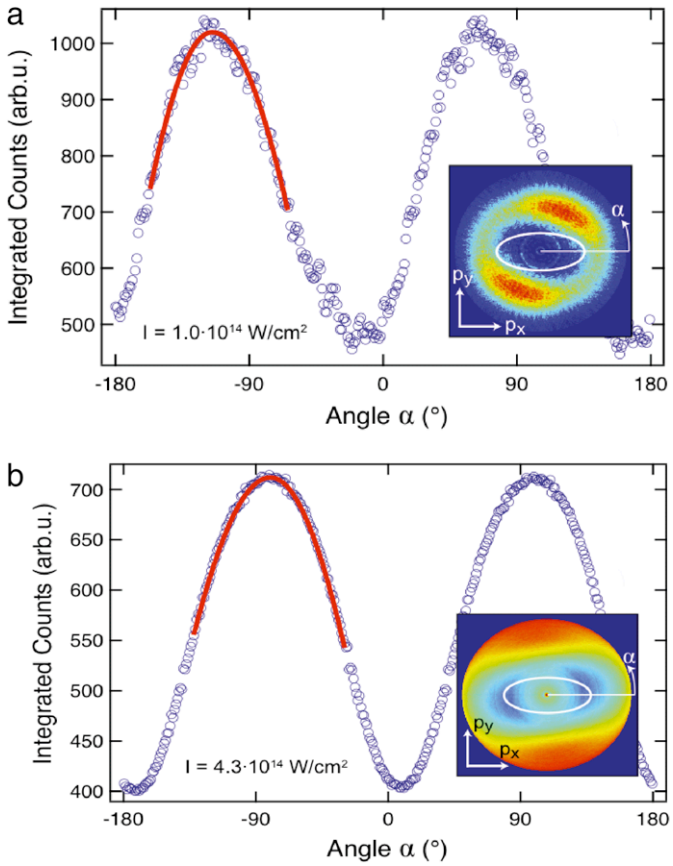

Fig. 9. Radially integrated electron momenta distributions. Tunnelling delay time is extracted from the measured angle for electrons located at the peak of this distribution. (a) Lower intensity and clockwise polarization; (b) Higher intensity and counter-clockwise polarization.

4.2. Basic principle

The principle of the attoclock has been described in some detail in prior publications [102,103]. In short, the attoclock definition of delay time relies on two independent measurements based on two observables. Observable 1 is the polarization axis of the elliptically polarized light and observable 2 is the electron momentum vector. The first observable determines time zero (defined as the peak of the laser field) and the second measures time the same way as time is measured with a normal watch. In the polarization plane the electron momentum vector is the "watch hand" and is fully defined with the polar coordinates (i.e. the radial and angular coordinate), where the angular coordinate directly gives the time information in full analogy to the "watch hand". The attoclock has the unique feature in that it uses close to circularly polarized light with the rotating electric field vector as the clock with a clearly defined rotation period and time zero.

The experimental observable is the electron momenta distributions in the plane of polarization, such as was shown in Fig. 4 of Section 2.4. The tunnelling delay time is extracted using angular streaking [9,25]. The idea of angular streaking is that final momentum of the electron can be used to obtain highly accurate information about when the electron first appears at the tunnel exit. This is already clear from Eq. (9) which shows a one to one correspondence between the final momentum and the time, t_0 when the electron appears at the tunnel exit, assuming the initial velocity of the electron, $\mathbf{v}(t_0)$, is known.

The tunnelling delay time is extracted for the centre of the distribution, corresponding to the most probable electron trajectory (see Fig. 9). This is done for a number of reasons. First, the initial velocity of the electron, $\mathbf{v}(t_0)$, for the most probable electron trajectory is known to be either zero (according to the ADK probability distribution [45]), or is given more generally (without adiabatic assumptions used by ADK or TIPIS) by the analysis of complex-valued trajectories that follow from the imaginary-time method [44] (sometimes referred to as the quantum orbit model [2] or the saddle point method). In this case, the initial conditions are approximated by Eqs. (7) and (12) Second, time zero is well-defined for the electron found at the centre of the momenta distribution and is given by the peak of the electric field. Finally, the peak of the momenta distribution is exceptionally robust to experimental noise, and in principle the accuracy is only limited by the accuracy of the Gaussian fit used to extract the peak.

To extract the centre of the momenta distribution, radial integration is used and the resulting distribution is fitted by a Gaussian, as shown in Fig. 9. Experimental tunnelling delay time, τ_{exp} is extracted from the experimentally measured angle,

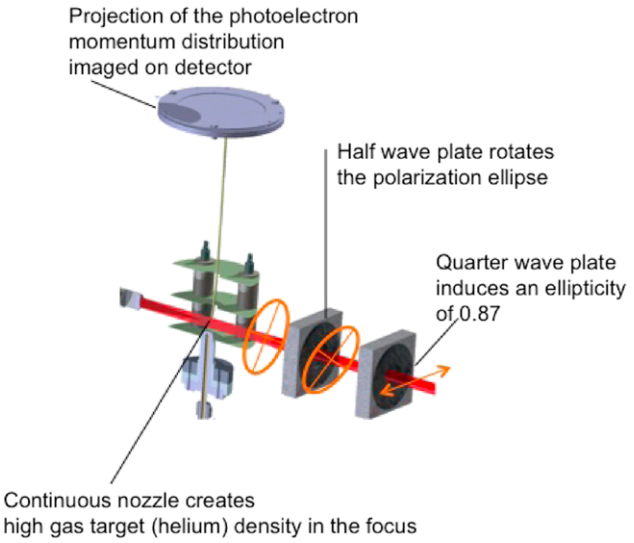

Fig. 10. Set-up of VMIS experiment.

θ_m, using the method of angular streaking [25]:

$$\tau_{exp} = \frac{\theta_i}{\omega} = \frac{(\theta_m - \theta_{Coul} - \theta_{str})}{\omega} \tag{60}$$

where θ_{Coul} is calculated using CTMC simulations, based either on TIPIS or the saddle point method, such as described in [38,42,44] (see Section 2.3). The streaking angle, θ_{str}, is 90 degrees if the electron appears in the continuum at the peak of the electric field, or $\theta_i = 0$, implying zero tunnelling delay time. For non-instantaneous delays, $\theta_{str} > 90$ degrees and depends strongly on ellipticity, such that,

$$\theta_{str} - \pi/2 \approx \frac{\left(1 - \epsilon^2\right)}{\epsilon}\theta_i \tag{61}$$

for sufficiently small θ_i. Unlike θ_{Coul}, the streaking angle is independent of intensity, but has a linear dependence on tunnelling time, since $\tau_{exp} = \theta_i/\omega$. In the following subsection, we describe recent and most complete attoclock measurements of tunnelling time, performed with two different experimental apparatus, COLTRIMS and VMIS.

4.3. The experiment

The most recent attoclock experiments [22] measure electron momenta distributions using two different experimental set-ups: a cold-target recoil-ion momentum spectrometer (COLTRIMS) and a velocity map imaging spectrometer (VMIS) [104], shown in Fig. 10. At lower intensities, attoclock measurements were performed by VMIS, allowing for access to a much wider intensity range than was previously possible. This was due to much higher target gas densities, compared to setups employing cold atomic beams [105]. Two-dimensional projections of the photoelectron momentum distributions were recorded in steps of two degrees covering 180 degrees (see Fig. 11). The three-dimensional momenta distribution, and thus the electron momenta distribution in the polarization plane, was retrieved by tomographic reconstruction [106]. More details on the VMIS experiment and the tomographic reconstruction method can be found in [107].

In COLTRIMS, the laser pulses were focused into a supersonic jet of atoms. Homogeneous electric and magnetic fields guide the ions and electrons to the opposite sides of the detector so that ion and electron momenta are measured in coincidence. In contrast to VMIS, the gas jet density is low so that the number of ion counts per pulse is typically less than one [26]. For measurements performed with the COLTRIMS, an additional source of uncertainty comes from the thermal spread of the gas jet. This results in a lower momentum resolution in the direction of jet propagation as compared to the transverse direction [36]. The thermal spread of the gas jet in COLTRIMS creates the dominant source of uncertainty of about 3 degrees, thus resulting in dominant contribution to the error bars in θ_m measurements. This is also the reason why the error bars on the recent VMIS measurements were much smaller than on the COLTRIMS measurements, allowing for a more accurate resolution of tunnelling delay time [22].

The laser pulses used in recent tunnelling time measurements [22] were generated by a Ti:Sapphire laser with a repetition rate of 10 kHz and pulse duration (full-width at half maximum) of 6.1 fs and central wavelength of 736 nm. The required ellipticity (or around $\epsilon = 0.87$) was created by a broadband quarter-wave plate. The polarization ellipse was rotated by a superachromatic half-wave plate. In the VMIS set-up, the ellipticity and the orientation of the major polarization axis

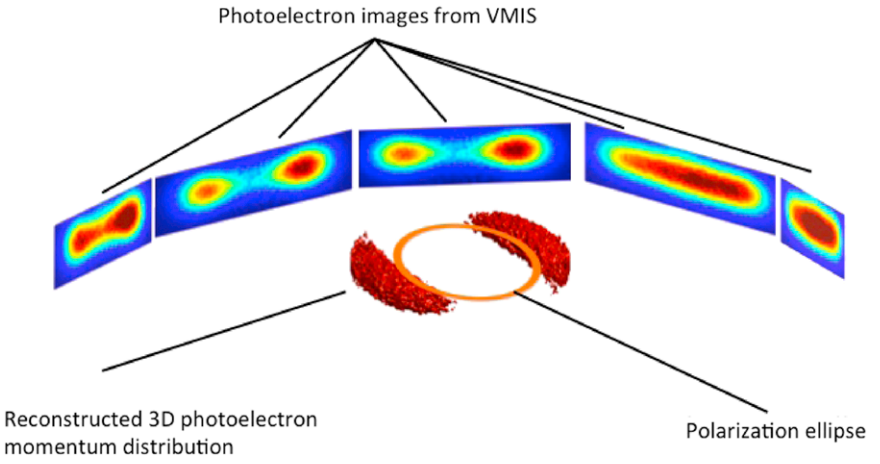

Fig. 11. Tomographic reconstruction method. Reconstruction of full 3-D electron momenta distribution using projections in momentum space.

was determined by recording the transmission through a cube polarizer as a function of the orientation of the rotating half wave plate [107]. In the COLTRIMS setup, a broadband quarter wave plate was employed to control the ellipticity while a broadband half wave plate was used to rotate the incoming linearly polarized light in order to align the major axis of the polarization ellipse along the time of flight axis.

4.4. Comparison of experiment to theory

In the limit of electron tunnelling from a bound state in a static electric field (corresponding to $\gamma \to 0$), the four tunnelling time definitions introduced in Section 3 can be implemented exactly. *The exact solution of the Schrödinger equation in this pure tunnelling (as opposed to multi-photon ionization) limit shows that all of these tunnelling times are finite* [22,69]. On the other hand, the use of a WKB approximation, or alternatively the saddle-point approximation, incorrectly predicts instantaneous phase-dependent tunnelling times (most prominent example being the Larmor time). The reason for this can be most easily seen by considering an elementary example of propagation of a plane wave through a rectangular barrier. In this case, the phase tunnelling times are well defined and non-instantaneous (see for example the appendix of [14]). However, as can be easily verified, the use of a WKB approximation will yield instantaneous phase-dependent tunnelling times by taking only a single decaying solution inside of the rectangular barrier and matching it to the fixed (with respect to barrier height) oncoming wave function. In other words, by using only a single solution, we can only match the wavefunctions at the boundary, not their derivatives, and therefore loose the ability to correctly express the phase as a function of barrier height at the tunnel exit. This in turn, will give an instantaneous Larmor time based on the definition in Eq. (27).

Similarly, in strong field ionization, the common procedure is to match a single saddle point solution to the field-free bound state wave function [49]. While this approximates well the absolute value of the transmission amplitude, it looses relevant information on the transmission phase, and hence predicts instantaneous phase tunnelling times, such as was found in [67]. Therefore, for computation of phase-dependent tunnelling time definitions, it is important that the full solution is taken inside the barrier and that the bound-state wavefunction is not approximated by a fixed field-free wavefunction, but is rather solved for the particular potential at the instance of tunnelling [22,69].

The experiment described in Section 4.3 explored a wide intensity range of about $0.73 - 7.5 \times 10^{14}$ W/cm^2 [22], corresponding to a significant variation in barrier width and a gamma such that $0.8 < \gamma < 2.5$, corresponding to a regime of "non-adiabatic tunnel ionization" [35]. This substantial variation of barrier width introduces a variation in the measured tunnelling time and allows for a detailed comparison with various definitions of tunnelling time introduced in Section 3. It was found in [22] that three of the tunnelling times, namely the Büttiker–Landauer, the Eisenbud–Wigner, and the Pollack–Miller were far too large to account for the attoclock measurements. In particular, these three times were on the order of two hundred attoseconds or more over the entire intensity range, while the attoclock measurements (although increasing slightly at lower intensities) were within 100 as.

Therefore, of the five times introduced in the prior section, only two showed agreement with the attoclock measurements: the Larmor time and the probability distribution of tunnelling times constructed using a Feynman path integral (FPI) formulation. As shown in Section 3, the Larmor time, τ_{LM}, can be expressed as an average, rather than a deterministic, quantity using the probability amplitudes constructed with the FPI approach. Therefore, the "correctness" of Larmor time for tunnelling would not exclude the existence of a probability distribution of tunnelling times.

The probability distribution of tunnelling times constructed using FPI approach is shown in Fig. 12 [22]. It has a long asymmetric tail that lengthens, along with an increase in the position of the peak as intensity decreases. This suggests that at lower intensities, both the duration of the tunnelling process and the uncertainty increase considerably. At all measured intensities, the FPI approach suggests that there is a non-negligible uncertainty associated with the duration of the tunnelling

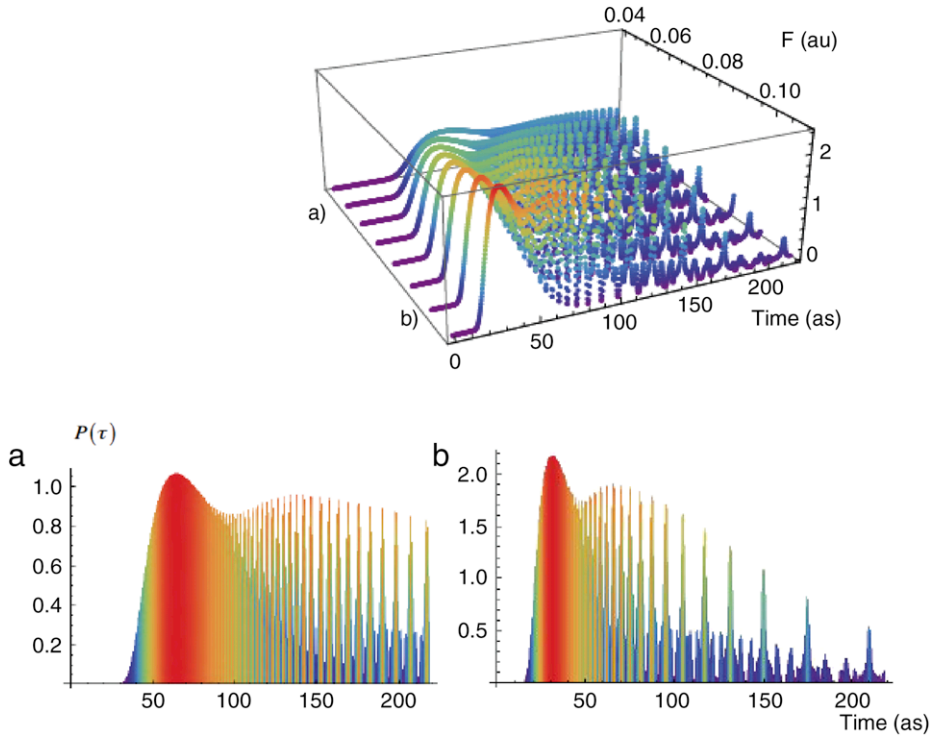

Fig. 12. Top: 3D probability distribution of tunnelling times constructed using the FPI approach, taken from [22]. (a) Probability distribution at Intensity 1.6×10^{14} W/cm^2. (b) Intensity 6.5×10^{14} W/cm^2.

process. In particular, the full-width-half-maxima (FWHM) of the distribution is larger or comparable to the "universal attosecond response to removal of an electron" of around 50 as, found computationally in [108].

5. Conclusion

The different definitions of tunnelling time introduced in Section 3 were developed for static potential barriers where the exit point is well-defined [12,14]. Therefore certain caution must be taken when applying these definitions to tunnelling in strong field ionization, where the barrier shape varies as a function of time. In particular, these definitions are most valid in the adiabatic limit, where the electric field of the laser varies sufficiently slowly *relative* to the tunnelling time these definitions predict (see Section 4.4). Because the Büttiker–Landauer and the Pollack–Miller times were comparable to the period of the laser field, the barrier could not assumed to be stationary during the tunnelling process, making the application of these definitions questionable in typical experimental regimes where $\gamma \sim 1$. Note that γ can be expressed as the ratio of the Keldysh or the Büttiker–Landauer tunnelling time to the period of the laser field. However, since the tunnelling time measured by the attoclock was actually less than 100 as, it could be assumed that the electric field stayed relatively constant during the tunnelling process, making it possible to exclude the Büttiker–Landauer, Eisenbud–Wigner, and Pollack–Miller times. For more rigorous future applications of various tunnelling time definitions to strong field ionization, one will need to extend the original definitions to include time-dependent potentials. This is a highly non-trivial task, since in the case of a time-dependent potential the exit point is not well-defined but depends on the tunnelling time itself. The possibility that tunnelling time may be a probabilistic rather than deterministic quantity further complicates matters.

As Section 3 reminds, the common definitions of tunnelling time can be viewed as expectation values, rather than deterministic quantities. In fact, such view is compatible with the quantum mechanical uncertainty that is associated with the tunnelling process. Moreover, as we show in Section 3, the four well-known tunnelling time definitions can be expressed as different averages using the Feynman path integral approach. It is not clear on purely theoretical grounds which one of those averages gives the "correct" tunnelling time. This view of tunnelling times as averages in turn implies that the time it takes an electron to tunnel is a probabilistic, rather than a deterministic process. The width of the probability distribution in this case represents the uncertainty associated with the tunnelling process, which may be more important for practical applications than the average duration of tunnelling. In particular, the existence of a probability distribution of tunnelling times, as opposed to a distinct tunnelling time, could add considerable uncertainty in the reconstruction of attosecond electron dynamics after strong field ionization. Many such reconstruction procedures rely on the assumption that the tunnelling process is deterministic and moreover instantaneous [3–5]. Hence the existence of a probability distribution

of tunnelling times would add an additional obstacle to achieving the desired attosecond temporal resolution to observe electron dynamics in "real time" [109,110].

Acknowledgements

This research was supported by the ERC advanced grant, NCCR MUST, funded by the Swiss National Science Foundation (SNSF), and an SNSF project grant. Our ultrafast activities are supported by the ETH Femtosecond and Attosecond Science and Technology (ETH-FAST) initiative as part of the NCCR MUST program.

References

[1] F. Krausz, M.Y. Ivanov, Ref. Mod. Phys. 81 (2009) 163.
[2] D. Shafir, et al., Nature 485 (2012) 343.
[3] O. Smirnova, et al., Nature 460 (2009) 972.
[4] E. Goulielmakis, et al., Nature 466 (2010) 739.
[5] A. Wirth, et al., Science 334 (2011) 195.
[6] M. Uiberacker, et al., Nature 466 (2007) 627.
[7] M. Meckel, et al., Science 320 (2008) 1478.
[8] H. Akagi, et al., Science 325 (2009) 1364.
[9] P. Eckle, et al., Science 322 (2008) 1525.
[10] M. Schultze, et al., Science 328 (2010) 1658.
[11] L.A. MacColl, Phys. Rev. 40 (1932) 621.
[12] R. Landauer, T. Martin, Rev. Modern Phys. 66 (1994) 217.
[13] G. Muga, R.S. Mayato, I. Egusquiza (Eds.), Time in Quantum Mechanics, in: Lecture Notes in Physics, vol. 734, Springer, Berlin, Heidelberg, 2008.
[14] E.H. Hauge, J.A. Stovneng, Rev. Modern Phys. 61 (1989) 917.
[15] R. Landauer, Nature 341 (1989) 567.
[16] M. Lein, Nature 485 (2012) 313.
[17] J. Zhao, M. Lein, Phys. Rev. Lett. 111 (2013) 043901.
[18] L.V. Keldysh, Sov. Phys.—JETP 20 (1965) 1307.
[19] M. Büttiker, R. Landauer, Phys. Rev. Lett. 49 (1982) 1739.
[20] H.A. Fertig, Phys. Rev. Lett. 65 (1990) 2321.
[21] N. Yamada, Phys. Rev. Lett. 93 (2004) 170401.
[22] A.S. Landsman, et al., arxiv:1301.2766.
[23] C.R. McDonald, G. Orlando, G. Vampa, T. Brabec, Phys. Rev. Lett. 111 (2013) 090405.
[24] M. Li, et al., Phys. Rev. Lett. 111 (2013) 023006.
[25] P. Eckle, et al., Nat. Phys. 4 (2008) 565.
[26] A.N. Pfeiffer, et al., Nat. Phys. 8 (2012) 76.
[27] M.Y. Ivanov, M. Spanner, O. Smirnova, J. Modern Optics 52 (2) (2005) 165.
[28] A.S. Landsman, U. Keller, Fifty Years of Optical Tunneling, J. Phys. B (2014) in press (special issue).
[29] A.S. Landsman, S.A. Cohen, M. Edelman, G.M. Zaslavsky, Commun. Nonlinear Sci. Numer. Simul. 10 (6) (2005) 617–642.
[30] A.S. Landsman, S.A. Cohen, A.H. Glasser, Phys. Plasmas 11 (3) (2004) 947.
[31] M. Lezius, V. Blanchet, D.M. Rayner, D.M. Villeneuve, A. Stolow, M.Y. Ivanov, Phys. Rev. Lett. 86 (1) (2001) 51.
[32] R. Boge, C. Cirelli, A.S. Landsman, S. Heuser, A. Ludwig, J. Maurer, M. Weger, L. Gallmann, U. Keller, Phys. Rev. Lett. 111 (2013) 103003.
[33] A.N. Pfeiffer, C. Cirelli, M. Smolarski, R. Dorner, U. Keller, Nat. Phys. 7 (2011) 428.
[34] P.B. Corkum, Phys. Rev. Lett. 71 (1993) 1994.
[35] G.L. Yudin, M.Y. Ivanov, Phys. Rev. A 64 (2001) 013409,d.
[36] A.N. Pfeiffer, C. Cirelli, A.S. Landsman, M. Smolarski, D. Dimitrovsky, L. Madsen, U. Keller, Phys. Rev. Lett. 109 (2012) 083002.
[37] A.S. Landsman, A.N. Pfeiffer, C. Hofmann, M. Smolarski, C. Cirelli, U. Keller, New. J. Phys. 15 (2013) 013001.
[38] V.D. Mur, S.V. Popruzhenko, V.S. Popov, J. Exp. Theor. Phys. 92 (2001) 777.
[39] I. Barth, O. Smirnova, Phys. Rev. A 84 (2011) 063415.
[40] S. Beiser, M. Klaiber, I. Yu Kiyan, Phys. Rev. A 70 (2004) 011402(R).
[41] S.P. Goreslavski, G.G. Paulus, S.V. Popruzhenko, N.I. Shvetsov-Shilovski, Phys. Rev. Lett. 93 (2004) 233002.
[42] A.M. Perelomov, V.S. Popov, M.V. Terentev, Sov. Phys.—JETP 50 (1966) 1393.
[43] V.S. Popov, Phys.-Uspekhi 47 (9) (2004) 855.
[44] V.S. Popov, Phys. Atom. Nucl. 68 (4) (2005) 686.
[45] M.V. Ammosov, N.B. Delone, V.P. Krainov, Sov. Phys.—JETP 64 (1986) 1191.
[46] C. Hofmann, A.S. Landsman, C. Cirelli, A.N. Pfeiffer, U. Keller, J. Phys. B: At. Mol. Opt. Phys. 46 (2013) 125601.
[47] A.S. Landsman, C. Hofmann, A.N. Pfeiffer, C. Cirelli, U. Keller, Phys. Rev. Lett. 111 (2013) 263001.
[48] L. Arissian, C. Smeenk, F. Turner, C. Trallero, A.V. Sokolov, D.M. Villeneuve, A. Staudte, P.B. Corkum, Phys. Rev. Lett. 105 (2010) 133002.
[49] R. Murray, W.K. Liu, M.Y. Ivanov, Phys. Rev. A 81 (2010) 023413.
[50] T. Nubbemeyer, K. Gorling, A. Saenz, U. Eichmann, W. Sandner, Phys. Rev. Lett. 101 (2008) 233001.
[51] H.R. Telle, et al., Appl. Phys. B 69 (1999) 327.
[52] F. Quere, Nat. Phys. 5 (2009) 93.
[53] A.S. Landsman, S.A. Cohen, A.H. Glasser, Phys. Rev. Lett. 96 (2006) 015002.
[54] S.A. Cohen, A.S. Landsman, A.H. Glasser, Phys. Plasmas 14 (2007) 072508.
[55] B. Dromey, et al., Nat. Phys. 2 (2006) 456.
[56] P.B. Corkum, F. Krausz, Nat. Phys. 3 (2007).
[57] L.D. Landau, E.M. Lifshitz, Quantum Mechanics, Vol. 3, Pergamon Press, 1965.
[58] H.R. Reiss, Phys. Rev. A 22 (1980) 1786.
[59] F.H.M. Faisal, J. Phys. B 6 (1973) L89.
[60] R.H. Fowler, L. Nordheim, Proc. R. Soc. 119 (781) (1928) 173.
[61] E.P. Wigner, Phys. Rev. 98 (1) (1955) 145.
[62] J.M. Dahlström, A. L'Huillier, A. Maquet, J. Phys. B: At. Mol. Opt. Phys. 45 (2012) 183001.
[63] K. Klünder, et al., Phys. Rev. Lett. 106 (2011) 143002.
[64] O. Smirnova, M.Y. Ivanov, Phys. Rev. Lett. 101 (2011) 213605.
[65] A. Kheifets, I. Ivanov, Phys. Rev. Lett. 105 (2010) 233002.
[66] C.H. Zhang, U. Thumm, Phys. Rev. A 84 (2010) 033401.

[67] L. Torlina, F. Morales, J. Kaushal, H. Muller, I. Ivanov, A. Kheifets, M. Ivanov, O. Smirnova, Conference Proceedings, HILAS, OSA, 2014.
[68] M. Klaiber, E. Yakaboylu, H. Bauke, K.Z. Hatsagortsyan, C.H. Keitel, Phys. Rev. Lett. 110 (2013) 153004.
[69] A.S. Landsman, et al., in preparation.
[70] Y. Aharonov, Z. Albert, L. Vaidman, Phys. Rev. Lett. 60 (1988) 1351.
[71] D. Bohm, Quantum Theory, Prentice-Hall, New York, 1951;
E.P. Wigner, Phys. Rev. 98 (1955) 145.
[72] A.I. Baz', Sov. J. Nucl. Phys. 4 (1967) 182.
[73] V.F. Rybachenko, Sov. J. Nucl. Phys. 5 (1967) 635.
[74] E. Pollak, W.H. Miller, Phys. Rev. Lett. 53 (1984) 115.
[75] N. Yamada, Phys. Rev. Lett. 93 (2004) 170401.
[76] D. Sokolovski, L.M. Baskin, Phys. Rev. A 36 (1987) 4606.
[77] Ph. Balcou, L. Dutriaux, Phys. Rev. Lett. 78 (1997) 851.
[78] C.R. Leavens, G.C. Aers, Solid State Commun. 63 (1987) 1107.
[79] C.R. Leavens, Found. Phys. 25 (2) (1995).
[80] M. Büttiker, Phys. Rev. B 27 (1983) 6178.
[81] M. Gell-Mann, J.B. Hartle, Proceedings of the 25th International Conference on High Energy Physics, World Scientific, Singapore, 1991.
[82] F.T. Smith, Phys. Rev. 118 (1960) 349.
[83] Ch. Spielmann, R. Szipöcs, A. Stingle, F. Krausz, Phys. Rev. Lett. 73 (1994) 2308.
[84] E.A. Galapon, Phys. Rev. Lett. 108 (2012) 170402.
[85] R.P. Feynman, A.R. Hibbs, Quantum Mechanics and Path Integrals, McGraw-Hill, New York, 1965.
[86] M. Dykman, I.B. Schwartz, A.S. Landsman, Phys. Rev. Lett. 101 (2008) 078101.
[87] D. Sokolovski, S. Brouard, J.N.L. Connor, Phys. Rev. A 50 (1994) 1240.
[88] D. Sokolovski, Phys. Rev. Lett. 79 (1997) 4946.
[89] G. Muga, R.S. Mayato, I. Egusquiza, Time in Quantum Mechanics, Vol. 1, in: Lecture Notes in Physics, vol. 734, Springer-Verlag, 2002.
[90] R. Feynman, The Feynman Lectures on Physics, Addison-Wesley, Boston, 1989.
[91] N. Yamada, Phys. Rev. Lett. 83 (1999) 3350.
[92] S. Boonchui, V. Sa-yakanit, Phys. Rev. A 77 (2008) 044101.
[93] H. Wiseman, New J. Phys. 9 (2007) 165.
[94] A.M. Steinberg, Phys. Rev. Lett. 74 (1995) 2405.
[95] T. Morita, T. Sasaki, I. Tsutsui, Prog. Theor. Exp. Phys. (2013) 053A02.
[96] C.A.A. de Carvalho, H.M. Nussenzveig, Phys. Rep. 364 (2002) 83–174.
[97] S. Kocsis, B. Braverman, S. Ravets, M.J. Stevens, R.P. Mirin, L.K. Shalm, A.M. Steinberg, Science 332 (2011) 1170.
[98] See IOP Physics World Number 1 breakthrough of 2011.
[99] L.A. Rozema, A. Darabi, D.H. Mahler, A. Hayat, Y. Soudagar, A.M. Steinberg, Phys. Rev. Lett. 109 (2012) 100404.
[100] D. Esteve, J.M. Martinis, C. Urbina, E. Turlot, M.H. Devoret, P. Grabert, S. Linkwitz, S. Physica Scr. T29 (1989) 121.
[101] A.M. Steinberg, P.G. Kwiat, R.Y. Chiao, Phys. Rev. Lett. 71 (1993) 708.
[102] A.N. Pfeiffer, C. Cirelli, M. Smolarski, U. Keller, Chem. Phys. 414 (2013) 84.
[103] L. Gallmann, C. Cirelli, U. Keller, Ann. Rev. Phys. Chem. 63 (2012) 447.
[104] D.H. Parker, A.T.J.B. Eppink, J. Chem. Phys. 107 (1997) 2357.
[105] O. Ghafur, et al., Rev. Sci. Instrum. 80 (2009) 033110.
[106] M. Wollenhaupt, et al., Appl. Phys. B - Lasers 95 (2009) 647.
[107] M. Weger, J. Maurer, A. Ludwig, L. Gallmann, U. Keller, Optics Express 21 (2013) 21981.
[108] J. Breidbach, L.S. Cederbaum, Phys. Rev. Lett. 94 (2005) 033901.
[109] O. Smirnova, M. Ivanov, Nat. Phys. 6 (2010) 59.
[110] S. Leone, et al., Nature Photon. 8 (2014) 162.